MICROSPHERE BASED OPTICAL BIOSENSORS

by

Şenol İşçi

BS, in Physics, Boğaziçi University, 2000

Submitted to the Institute of Biomedical Engineering
in partial fulfillment of the requirements
for the degree of
Master of Science
in
Biomedical Science

Boğaziçi University
2003

ACKNOWLEDGMENTS

I am deeply grateful to my thesis supervisors, Assoc. Prof. Cengizhan Öztürk and Assoc. Prof. Ali Serpengüzel for their kind academic support, supervision and motivation during this research with endless tolerance and patience.

I would like to thank my thesis committee members Assoc. Prof. Mehmed Özkan, Asst. Prof. Murat Gülsoy, and Asst. Prof. Ata Akın for their patience in reading the thesis drafts carefully and for making valuable suggestions.

I am deeply grateful to Adnan Kurt for his continuous support and invaluable advice, to Temel Bilici, Yiğit Ozan Yılmaz, and İbrahim İnanç for their close friendship.

I would like to thank Prof. Selim Küsefoğlu for providing me with the chemical procedures for the glass surface modifications. My thanks also go to Asst. Prof Adem Levent Demirel for testing the coatings of glass samples and for his useful suggestions.

I would also like to thank Koç University Microphotonics Research Laboratory, The Scientific & Technical Research Council of Turkey (TÜBİTAK), and The European Office of Aerospace Research and Development (EOARD) for sponsoring my research.

Finally, I would like to thank my family for always being with me.

ABSTRACT

MICROSPHERE BASED OPTICAL BIOSENSORS

Optical microsphere resonators have recently utilized in quantum optics, laser science, spectroscopy, and optoelectronics and attracted increasing interest due to their unique optical properties. Microspheres possess high quality factor (Q-factor) optical morphology dependent resonances, and have relatively small volumes. Q-factor can be defined as how sharp morphology dependent resonance in the elastic scattering spectrum. High-Q morphology dependent resonances are very sensitive to the refractive index change and microsphere uniformity. These tiny optical cavities, whose diameters may vary from a few to several hundred micrometers, have resonances with reported Q-factors as large as 3×10^9. Due to their sensitivity, morphology dependent resonances of microspheres are also considered for biosensing applications. For instance, binding of a protein or other biomolecules can be monitored by observing the wavelength shift of morphology dependent resonances. A biosensor, based on this optical phenomena, can even detect a single molecule if a good system design is achieved.

In this work, elastic scattering spectra from the microspheres of different materials are experimentally obtained and morphology dependent resonances are observed. Furthermore, the morphology dependent resonances of microspheres for biosensor applications were studied theoretically.

Keywords: Biosensor, Microsphere, Morphology Dependent Resonances.

ÖZET

MİKROKÜRE OPTİK BİYOALGILAYICILAR

Optik mikroküre çınlaçları kuvantum optiğinde, lazer biliminde, spektroskopide ve optoelektronik alanlarında kullanılmakta ve benzersiz optik özelliklerinden dolayı hergeçen gün ilgi toplamaktadır. Mikroküreler, yüksek kalite faktörlü yapısal çınlamalara ve küçük hacimlere sahiptirler. Kalite faktörü, elastik saçılma tayfında yapısal çınlamaların ne kadar keskin olduğu ile ilişkilendirilir. Yüksek kalite faktörlü yapısal çınlamalar, kırılma indislerindeki ve mikrokürenin küreselliğindeki değişimlere çok duyarlıdırlar. Yarıçapları 5 mikrometreden 500 mikrometreye kadar değişen bu küçük optik çınlaçların, 3×10^9 gibi yüksek kalite faktörüne ulaştığı bildirilmiştir. Bu tür yüksek hassaslığa sahip olduklarından dolayı mikrokürelerin yapısal çınlamalarının, biyoalgılayıcı uygulamalarında kullanılması mümkündür. Örnek olarak, bir proteinin yada diğer biyomoleküllerin mikroküre yüzeyine bağlanması, yapısal çınlamaların frekansındaki kaymalar gözlenerek tespit edilebilir. Bu optik olaya dayalı çalışacak bir biyoalgılayıcının uygun bir tasarımla tek bir molekül tespiti yapababilmesi de teorik olarak mümkündür.

Bu çalışmada, çeşitli malzeme yapısındaki mikrokürelerden, deneysel olarak elastik saçılım tayfları elde edilmiş ve yapısal çınlamalar gözlemlenmiştir. Ayrıca, optik çınlaç olarak mikroküreler, yapısal çınlamalar ve bu optik olayın, biyoalgılayıcı uygulamalarında nasıl kullanılabileceği incelenmiştir.

Anahtar Sözcükler: Biyoalgılayıcı, Mikroküre, Yapısal çınlama

TABLE OF CONTENTS

LIST OF FIGURES

LIST OF TABLES

LIST OF SYMBOLS

a	Radius of the microsphere
a_n	TE expansion coefficient of the scattered E field
α	Polarizability
α_{ex}	Excess polarizability
a_ℓ	Roots of the Airy function
b	Impact parameter
b_n	TM expansion coefficient of the scattered M field
$\Delta\lambda$	Mode spacing in wavelength
$\delta\omega$	Frequency shift of a MDR
Δx	Mode spacing in size parameter
ΔW	Molecular energy shift
E	Electric field
ϵ	Permittivity of the medium
E	the energy stored in the MDR
E_0	Steady state energy in the MDR
$\hbar$	Planck's constant divided by 2π
$h_n(x)$	Spherical Hankel function
I_i	Incident beam intensity
$j_n(x)$	Spherical Bessel function
k	Wavenumber
ℓ	Mode order
λ	Wavelength
m	Azimuthal mode number
m	Refractive index
μ	Permeability of the medium
n	Mode number
ω	MDR angular frequency
p	Momentum of the photons

P_i	Power coupled into the MDR
Q-factor	Quality Factor
Q_0	The intrinsic Q-factor of the μ-sphere
Q_f	The Q-factor of the μ-sphere-OFHC system
Q_T	The total Q-factor the MDR's for the μ-sphere-OFHC system
σ	Scattering cross section
σ_{total}	Total scattering cross section
σ_p	Surface density of biomolecules
τ	Photon lifetime of a wave
θ_{inc}	Angle of incidence
θ_c	Critical Angle
x	Size parameter

LIST OF ABBREVIATIONS

API	Application Programming Interface
BSA	Bovine Serum Albumin
DFB	Distributed Feedback Laser
DNA	Deoxyribo Nucleic Acid
FWHM	Full Width at Half Maximum
GLMT	Generalized Lorenz Mie Theory
GPIB	General Purpose Interface Bus
LDC	Laser Diode Controller
MDR	Morphology Dependent Resonance
μ-sphere	Microsphere
OFHC	Optical Fiber Half Coupler
OMM	Optical Multimeter
PMT	Photomultiplier Tube
TE	Transverse Electric
TIR	Total Internal Reflection
TM	Transverse Magnetic
WGM	Whispering Gallery Mode

1. INTRODUCTION

1.1 Motivation and Objectives

Optical biosensors represent the second major family of biosensors, after electrochemical biosensors to have been exploited in genomics and proteomics studies, and a lot of research is going on devoicing new biosensors, which are based on optical methods. This has been made possible by progress in fiber-optic technology, laser miniaturization and the reproducible manufacture of prisms and waveguides. Some optical biosensors are best seen as miniaturized versions of "traditional" spectrophotometers, while others are based on new, integrated-optic methods such as evanescent waves and light-addressable potentiometric semiconductors [1]. In recent years genetic analysis applications have been a major focus for optical sensors. Although miniaturized high-density arrays of oligonucleotide probes, DNA chip, are proving to be powerful tools for DNA sequencing, DNA chip fabrication methods remain a challenge for creating cost-effective devices. An alternative method to biochip is based on optical methods, which sense binding of DNA probes to microspheres.

Optical microsphere resonators with morphology dependent resonances (MDR's) or whispering-gallery modes (WGM's) have attracted an increasing interest in quantum optics, laser science, spectroscopy, biosensor applications, and optoelectronics [2]. In the ray optics view, light at certain frequencies, which is propagating around the microsphere confined by an almost total internal reflection (TIR), creates MDR's. After travelling around the microsphere, the light beam returns to its initial position in phase. Resonance frequency,(or wavelength) locations of the peaks in the resonance spectrum depends on the size, shape, and refractive index of the microspheres. A frequency shift of the MDR's when radius or refractive index of the sphere changes, makes possible the utilization of the MDR's of microspheres in detecting trace amounts of chemicals and biological molecules. These sensors would offer ultrahigh sensitivity, and in some cases, enough sensitivity to detect single molecules [3].

The aim in this thesis is to study the possible use of microspheres as a biosensor agents to detect different molecules such as proteins and DNA sequences. These systems are still on a basic research level, and this topic gained a great interest among the researchers. Recently, researchers studying this phenomenon have obtained preliminary results. Arnold *et al.* showed the shift of MDR's of microspheres by protein adsorption [4, 5]. Many experimental studies are still required to enhance the use of microspheres as biosensors. The questions that need answers are: (i) possibility of using this new optical biosensing technique in genomic studies, (ii) sensitivity, (iii) specificity of microspheres as biosensors, and (iv) possibility of biosensor microsphere arrays.

1.2 Outline of The Thesis

Chapter 1 covers the motivation and objectives of the thesis. Chapter 2 includes the theory and the properties of morphology dependent resonances of microspheres. In chapter 3, the off-axis Gaussian beam method for excitation of morphology dependent resonances, which is used in the experiments, is described. The experimental and simulation results of the excitation of morphology dependent resonances are presented. Chapter 4 covers the perturbation theory, which explains how the morphology dependent resonances shift when a biomolecule interacts with the microsphere. The biosensing applications are discussed, and some examples are given . In chapter 5, Immobilization of biomolecules onto the microspheres are described, which is a crucial part affecting the sensitivity and selectivity properties of microsphere based biosensing. Also, how glass surfaces can be modified to build a functionalized microsphere biosensor transducer is experimentally shown.

2. MORPHOLOGY DEPENDENT RESONANCES

Optical microsphere (μ-sphere) resonators have recently attracted an increasing interest in quantum optics, laser science, spectroscopy, biosensor technology, and optoelectronics. μ-spheres possess high quality factor (Q-factor) optical morphology dependent resonances (MDR's) and have relatively small volumes [6, 7]. Q-factor gives information about the lifetime and linewidth of a MDR. High-Q MDR's are very sensitive to the refractive index change and μ-sphere uniformity. These tiny optical cavities, whose diameters may vary from a few to several hundred micrometers, have MDR's with reported Q-factors as large as 3×10^9 [8]. There has been extensive research on the MDR's, which are also called whispering gallery modes (WGM's): low threshold lasing from Nd-doped silica μ-spheres [9] , polymer μ-sphere lasers [10] and, Raman μ-sphere lasers [11] have been demonstrated. Additionally, strain tunable μ-sphere oscillators [12], add-drop filters [13] have been realized. Thermo-optical switching [14] can also be applied to μ-spheres for frequency control in optical communication applications. Due to their great sensitivity, MDR's of microspheres are also considered for biosensing applications [3, 4, 5, 15].

2.1 Ray and Wave Optics

The most intuitive picture describing the optical resonances of microspheres is based upon ray and wave optics. A ray of light propagating within a sphere of radius a and index of refraction $\mathbf{m}(\omega)$ will undergo total internal reflection (TIR), if the angle of incidence with the dielectric interface, θ_{inc}, is $\geq \theta_c = \arcsin(1/m(\omega))$. The rays of a MDR have the property that all subsequent bounces have the same angle of incidence. Hence, the light is confined to a band within a great circle of the sphere. A "caustic region" can be defined as an inner-sphere region within the dielectric sphere to which the propagating and bouncing rays are tangent. A small fraction of the light on an MDR is contained in the caustic sphere (see Fig. 2.1). For the case of a perfect sphere,

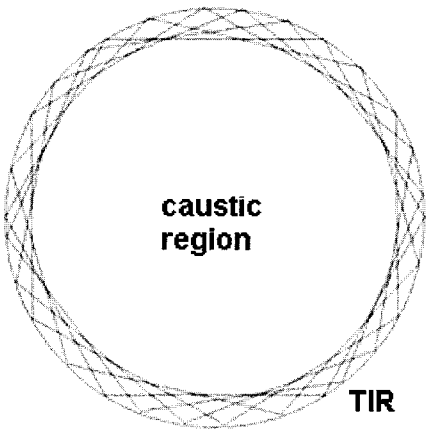

Figure 2.1 Schematic of the total internal reflection (TIR) of rays and the caustic region in the μ-sphere.

geometric optics does not provide a method for the light to escape as long as $\theta_{inc} \geq \theta_c$. This problem is resolved by wave theory; diffraction due to the curvature of the sphere surface causes light to leak tangentially from the sphere rim. For the case of a sphere with circumference $2\pi a \gg \lambda$ and light propagating with $\theta_{inc} \approx 90^o$, the resonance condition is that the optical path length is approximately equal to the circumference of the sphere. The permitted limits of n wavelengths in the dielectric is the path length for one roundtrip with wavelengths for waves that are either confined mostly within the dielectric ($\lambda/\mathbf{m}(\omega)$) or extended mostly into the surrounding air (λ) [16]:

$$\frac{2\pi a}{\lambda} \leq n \leq \frac{2\pi a}{\lambda/\mathbf{m}(\omega)}. \tag{2.1}$$

The dimensionless size parameter is defined as:

$$x = 2\pi a/\lambda, \tag{2.2}$$

Rays of the plane wave that tangentially strike the sphere surface can excite MDR's, only if λ satisfies the resonance condition of Eq. 2.3.

$$x \leq n \leq \mathbf{m}(\omega)x \tag{2.3}$$

The phase-matching condition for the $n = \mathbf{m}(\omega)x$ MDR and the external wave corresponds to the case, where an internal ray completes one roundtrip as the $n\lambda$ of the plane wave reaches the sphere surface. The integer n can be identified as the angular momentum of the MDR by equating

$$\hbar n \approx ap \approx a\hbar k \tag{2.4}$$

for the case of near-glancing incidence of the ray ($\theta_{inc} \geq \theta_c$), where $\hbar$ is the Planck's constant divided by 2π, p is the momentum of photons, and k is the wavenumber defined as $2\pi/\lambda$.

If the normal to the MDR orbit is inclined at an angle θ with respect to the z-axis, the z-component of the angular momentum quantum number affiliated with the angular momentum quantum number of the MDR is,

$$m = n\cos\theta. \tag{2.5}$$

For a perfect sphere, all of the m modes are degenerate (with $2n+1$ degeneracy). The degeneracy is lifted when the cavity is axisymmetrically (along the z-axis) deformed from sphericity. For such distortions the integer values for m are $\pm n, \pm(n-1), ...0$, where the degeneracy remains, because the MDR's are independent of the circulation direction, i.e., clockwise or counterclockwise. Highly accurate measurements of the clockwise and counterclockwise circulating m-mode frequencies reveal a splitting due to internal backscattering, that couples the two counterpropagating modes [17].

In plane-wave illumination, the great-circle orbit of the rays need not be confined to the x-y plane (e.g., the equatorial plane). The curvature of the illuminated face

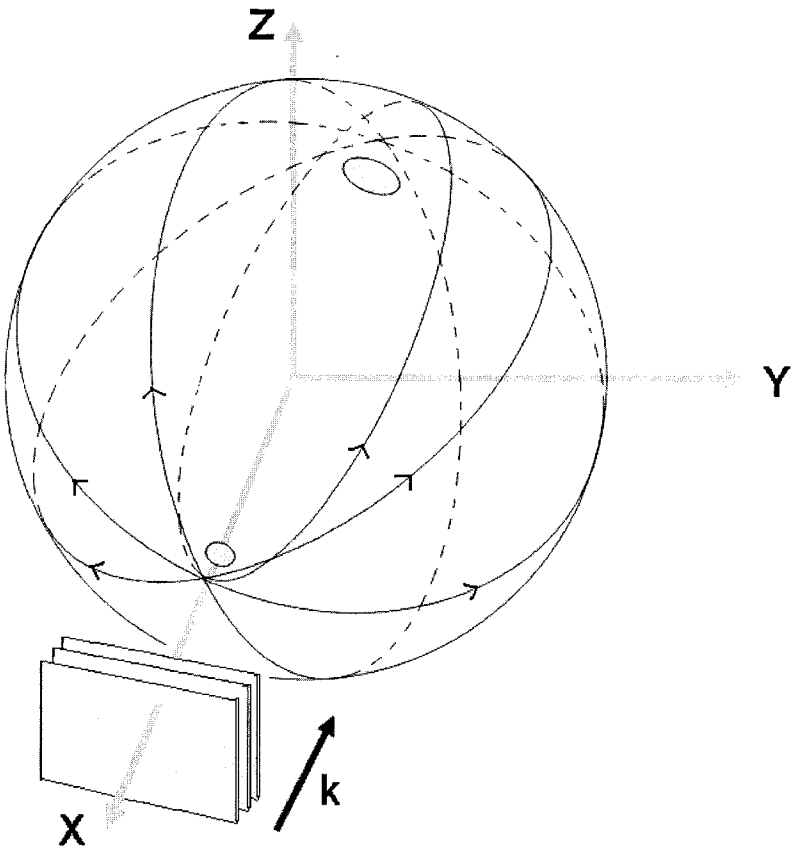

Figure 2.2 Circular paths of MDR's and focused spots for a plane-wave illumination geometry.

focuses the incident light to a hot spot with length $\sim 0.1a$ and width $\sim \lambda/2$ within the shadow face of the μ-sphere (see Fig. 2.2). Subsequent reflections lead to a weaker hot spot near the illuminated face. The intensity of light in the main spot can be greater than 100 times the intensity of the incident field, for lossless spheres with $x \gg 10$ [16]. The hot spots can serve as pumping regions for nonlinear optical processes and lasing [18].

The ray and wave optics description of light interaction with a μ-sphere has several limitations: it cannot explain escape of light from a MDR for perfect spheres. Furthermore, ray and wave optics provides no possibility for incident light to couple into a MDR, and the polarization of light is not taken into account. Finally, the radial character of the optical modes cannot be determined. All of these issues are explained

by the Maxwell wave equations with appropriate boundary conditions.

2.2 Electromagnetic Theory

A complete description of the interaction of light with a dielectric is given by the electromagnetic theory. The spherical geometry suggests expanding the fields in terms of vector spherical harmonics. Characteristic equations for the MDR's are derived by requiring continuity of the tangential components of both the electric and magnetic fields at the boundary of the dielectric sphere and the surrounding medium. Internal-intensity distributions are determined by expanding the incident wave (plane-wave or focused beam), internal field, and external field, all in terms of vector spherical harmonics and again imposing appropriate boundary conditions.

The MDR's of a μ-sphere are analyzed by the localization principle [19] and the generalized Lorenz-Mie theory (GLMT) [20, 21, 22] . Each MDR is characterized by a mode number n and a mode order ℓ. The mode number n gives the number of maxima between 0^o and 180^o degrees in the angular distribution of the energy of the MDR. The radial mode order ℓ indicates the number of maxima in the internal electric field distribution in the radial direction. Each MDR of the μ-sphere also has an azimuthal angular dependence from 0^o to 360^o, which is labelled with an azimuthal mode number m. However, for spheres, MDR's differing only in azimuthal mode number have identical resonance frequencies [23]. The characteristic eigenvalue equations for the natural resonant frequencies of dielectric μ-spheres have been solved in homogeneous surroundings. For the transverse electric (TE) and the transverse magnetic (TM) MDR's, continuity of the tangential electric and magnetic fields at the dielectric/air interface for a mode number n requires the following [24]:

$$\frac{[\mathbf{m}xj_n(\mathbf{m}x)]'}{j_n(\mathbf{m}x)} = \frac{[xh_n^{(1)}(x)]'}{h_n^{(1)}(x)} \tag{2.6}$$

$$\frac{[\mathbf{m}j_n(\mathbf{m}x)]'}{\mathbf{m}^2 j_n(mx)} = \frac{[xh_n^{(1)}(x)]'}{h_n^{(1)}(x)} \tag{2.7}$$

where $\mathbf{m}$ is the ratio of the refractive index of dielectric μ-sphere to that of the surrounding medium. The size parameter x is defined as $2\pi a/\lambda$, where λ is the wavelength in the surrounding medium, and a is the radius of the μ-sphere. In Eq.2.6 and 2.7 , $j_n(x)$ and $h_n^{(1)}(x)$ are the spherical Bessel and the Hankel functions of the first kind, respectively. The prime (') denotes differentiation with respect to the argument. The transcendental equation is satisfied only by a discrete set of characteristic values of the size parameter, $x_{n,\ell}$, corresponding to the radial ℓ^{th} root for each angular n [24].

2.2.1 Elastic Light Scattering

The elastically scattered field can be written as an expansion of vector spherical wave functions with TE coefficients (a_n) and TM coefficients (b_n) for a plane wave incident on a dielectric μ-sphere. The scattered field becomes infinite at complex frequencies $\omega_{n,\ell}$ corresponding to the complex size parameters $x_{n,\ell}$ at which, a_n and b_n become infinite. a_n coefficients are associated with $\mathrm{TE}_{n,\ell}$ MDR's specified by Eq. 2.8. Similarly, b_n coefficients are associated with the $\mathrm{TM}_{n,\ell}$ MDR's as specified by Eq. 2.9 [24, 25]. The expansion coefficients a_n and b_n are given by:

$$a_n = \frac{j_n(x)[mxj_n(mx)]' - m^2 j_n(mx)[xj_n(x)]'}{h_n^2(x)[mxj_n(mx)]' - m^2 j_n(mx)[xh_n^2(x)]'} \tag{2.8}$$

$$b_n = \frac{j_n(x)[mxj_n(mx)]' - j_n(mx)[xj_n(x)]'}{h_n^2(x)[mxj_n(mx)]' - j_n(mx)[xh_n^2(x)]'} \tag{2.9}$$

where j_n and $h_n^{(2)}$ are the spherical Bessel and Hankel functions of the second kind, respectively [26].

The MDR's of the μ-sphere occur at the zeros of the denominators of a_n and b_n coefficients. These poles, which are complex, occur at discrete values of the complex size parameter x. The modes are nonradiative for real frequencies, and hence the

modes are virtual and the resonance frequencies are complex. The real part of the pole frequency is close to the real MDR frequency [26]. The imaginary part of the pole frequency determines the linewidth of the MDR.

The natural MDR frequencies of $TE_{n,l}$ and $TM_{n,l}$ modes are given by [26, 24]:

$$\omega_{n,\ell} = \frac{x_{n,\ell}}{a\sqrt{\mu\epsilon}} \tag{2.10}$$

where μ is the permeability, and ϵ the permittivity of the surrounding lossless medium. Thus the equation above defines the complex frequencies at which, a dielectric μ-sphere will resonate in one of its MDR's [24]. The full width at half maximum(FWHM) of the resonance, denoted $\Delta x_{n,\ell}$ or $\Delta\omega_{n,\ell}$, is twice the imaginary part of $x_{n,\ell}$.

Q-FACTOR: The quality factor, Q, of a resonance is defined as

$$Q = \frac{Re(x_{n,\ell})}{2Im(x_{n,\ell})} = \frac{\omega_{n,\ell}}{\Delta\omega_{n,\ell}} = \omega_{n,\ell}\tau \tag{2.11}$$

where τ is the lifetime of a wave on an MDR. In a perfectly smooth homogeneous lossless sphere the Q values are limited by diffractive leakage losses and can be as high as 10^{100}. In reality, volume inhomogeneities, surface roughness, and absorption restrict the maximum Q values to be less than 10^{10}. Local or global shape deformations and nonlinear effects can further reduce the maximum Q value.

For frequencies near an MDR, the electric field inside the cavity varies as

$$\mathbf{E}(t) = \mathbf{E}_0 exp(-i\omega_0 t - \frac{\omega_0}{2Q}t). \tag{2.12}$$

The decay term leads to a broadening of the resonance linewidth, giving a Lorentzian lineshape for the energy distribution

$$|\mathbf{E}(\omega)|^2 \propto \frac{1}{(\omega - \omega_0)^2 + (\omega_0/2Q)^2} \tag{2.13}$$

For a given mode number, n the ℓ= 1 modes have the highest Q (smallest Δx), with a peak intensity located closest to the surface and the evanescent wave penetrating shortest into the surrounding medium. As ℓ increases, the Q value decreases, the peak intensity moves away from the surface, and the evanescent wave penetration into the surrounding medium increases. For a fixed radial mode order ℓ, modes with higher angular momentum or higher mode number n have higher Q values.

MDR POSITION: For spheres with large x, several expressions are derived to determine the spectral location, separation, and width of MDR's. The positions of MDR's are approximated by [27, 28]:

$$\mathbf{m}(\omega)x_{n,\ell} = \upsilon + 2^{-1/3}\alpha_\ell \upsilon^{1/3} - \frac{P}{\rho} + (\frac{3}{10}2^{-2/3})\alpha_\ell^2 \upsilon^{-1/3} \tag{2.14}$$

$$-\frac{2^{-1/3}P(\mathbf{m}^2(\omega) - 2P^2/3)}{\rho^3}\alpha_\ell \upsilon^{-2/3} + O(\upsilon^{-1})$$

where P= $\mathbf{m}(\omega)$ for TE modes, P=$1/\mathbf{m}(\omega)$ for TM modes, $\upsilon = n+1/2$, $\rho^2 = \mathbf{m}^2(\omega) - 1$ and α_ℓ are the roots of the Airy function.

MDR SEPARATION: The separation between resonances $\Delta x_{n,l}$ is more useful than the absolute mode positions to determine the approximate sphere size and approximating mode numbers. Asymptotic analysis gives [28]

$$\mathbf{m}(\omega)\Delta x_{n,\ell} = 1 + \frac{2^{-1/3}}{3}\alpha_l \upsilon^{-2/3} - \frac{2^{-2/3}}{10}\alpha_l^2 \upsilon^{-4/3} \tag{2.15}$$

$$+[\frac{2^{2/3}}{3}\frac{P(\mathbf{m}^2(\omega) - 2P^2/3)}{\rho^{4/3}} - \frac{2^{-1/3}}{9}]\alpha_l \upsilon^{-5/3} + O(\upsilon^{-2}).$$

Although Eq. 2.15 is more accurate, a simple approximation to Δx is given by [29]

$$\Delta x = \frac{tan^{-1}[(\mathbf{m}(\omega)x/n)^2 - 1]^{1/2}}{n[(\mathbf{m}(\omega)x/n)^2 - 1]^{1/2}} \qquad for\ |x - n| \gg 1/2 \tag{2.16}$$

$$\Delta x = \frac{tan^{-1}\rho}{\rho} \qquad for\ x/n\ 1$$

MDR DENSITY: An approximation to the mode density of high-Q MDR's, which is defined as the number of resonance modes per frequency or size-parameter interval, is [30]

$$MDR\ density = \frac{x\rho^2(\rho - tan^{-1}\rho)}{\pi}. \tag{2.17}$$

Equation 2.17 implies that the mode density increases rapidly as the refractive index increases.

2.2.2 Spatial Distribution of MDR's

The spatial distribution of MDR internal intensities can give further physical insight into the properties of MDR's. Figure 2.3 shows the internal intensity distribution in the equatorial plane for a $TE_{12,2}$ mode of a sphere with index of refraction ratio $\mathbf{m}(\omega) = 2.5$. Obviously, $n = 12$ x 2 intensity peaks are around the equator,

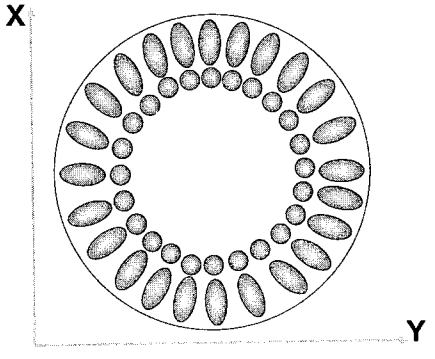

Figure 2.3 Internal-intensity distribution in the equatorial plane for a TE MDR with $n = 12$, $\ell = 2$.

corresponding to $n = 12$ wavelengths within the circumference and, to an effective angular momentum quantum number of 12. There are $\ell = 2$ intensity peaks along the μ-sphere radius.

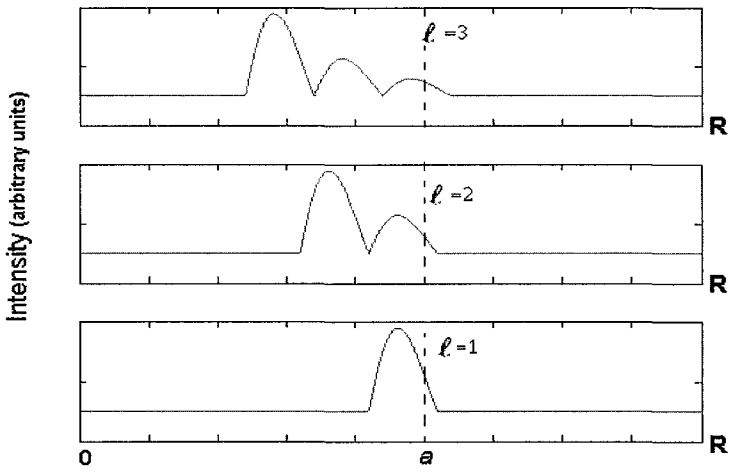

Figure 2.4 Typical illustration of angle-averaged intensity distribution profile along the radial direction for MDR's ℓ=1, 2, and 3 with same n.

As the mode order increases, number of peaks in the internal intensity profile increases, corresponding to the mode order, and the highest peak is located at the most inner side in the radial direction. An illustration of the angle-averaged radial intensity distribution for the same mode number with $\ell = 1, 2, 3$ is shown in Fig. 2.4.

The dependence of the internal intensity distribution on the azimuthal mode number m is depicted in Fig. 2.5, in which the angular internal intensity distribution is

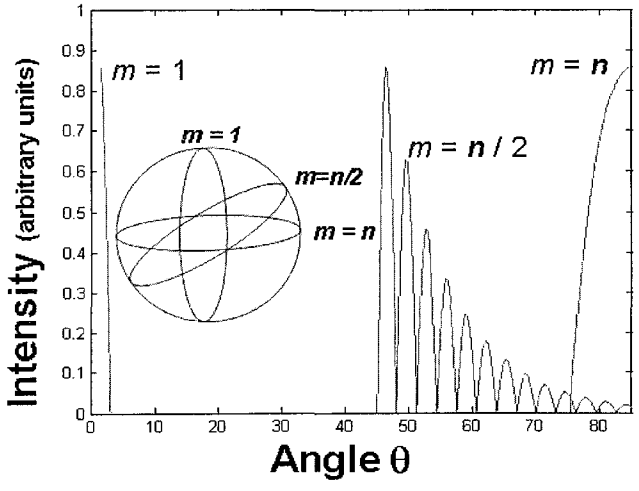

Figure 2.5 Typical illustration of internal-intensity distribution as a function of θ for TE MDR's with m = 1, n/2, and n.

a function of θ. Three MDR's for $m = 1$, n/2, and n are illustrated as the angle θ varies from 0^o to 90^o. These MDR's have the same resonance frequency, but the maximum intensity for each m is inclined at an angle $\theta = sin^{-1}(m/n)$. The maximum intensity peak agrees with the ray optics picture of an m-mode circulating in a confined orbit inclined at $\theta = sin^{-1}(m/n)$ and with its normal inclined at an angle $\theta = cos^{-1}(m/n)$.

2.2.3 Coupling to MDR's

Several methods can be used for exciting MDR's. The simplest case is plane-wave illumination. To improve the input coupling of the incident pump and the MDR, a focused Gaussian beam can be aimed at the equatorial edge of a sphere. The interaction of focused Gaussian beams with dielectric spheres was studied both theoretically [31, 32, 21, 22] and experimentally [33]. By focusing inside the sphere and away from the edge, even if the wavelength of the incident light corresponds to an MDR, the internal intensity distribution approximately preserves the Gaussian profile except for the refraction and reflection at the μ-sphere surface [34, 35].

A way to excite an MDR is to use evanescent coupling with a prism, stripped optical fiber, or partially unclad optical fiber half coupler (OFHC) [7, 36, 37]. It is easier to match the wavevector of the evanescent field of the MDR with that of the prism or stripped fiber. Near equatorial modes (m$\approx$n) are excited by placing the microsphere equator in the evanescent field of the fiber. The coupling efficiency is typically less than 20% [16]. The fiber coupling method has many potential applications in electro-optics and optical communications.

3. OBSERVATION OF MORPHOLOGY DEPENDENT RESONANCES

Efficient coupling to MDR's requires great attention for most of the applications. The greatest impediment to use the μ-sphere resonators in practical optical devices has been the difficulty of efficiently coupling light in and out of the μ-spheres. Efficient coupling to MDR's not only requires the adjustment of the frequency of the excitation beam to a MDR but also the excitation beam should have an angular momentum (with respect to the center of the μ-sphere), which matches the angular momentum of the MDR. This last condition is not met with a free propagating (plane-wave) beam, even if it is focused near the edge of the μ-sphere [7, 12, 33]. For plane-wave illumination, the internal intensity is concentrated along the principal diameter near the front and the back surfaces of the μ-sphere. If the incident plane wave is resonant with a MDR (i.e., on resonance), there will be, in addition, a uniform intensity distribution within the rim of the μ-sphere in the volume determined by the MDR. However, if an off-axis Gaussian beam is used at a resonant wavelength, the internal intensity is distributed only within the rim of the μ-sphere in the volume determined by the MDR and is no longer concentrated near the front and the back surfaces of the μ-sphere (see Fig. 3.1) [38, 18]. Therefore, evanescent coupling with a resonant off-axis Gaussian beam provides efficient excitation of the MDR's of a μ-sphere more uniformly and more efficiently than does a plane wave [38].

3.1 Gaussian Beam Excitation

Serpengüzel *et al.* have proposed and experimentally proved the off-axis morphology dependent resonance excitation [7, 38]. It can be depicted as the interaction of the μ-sphere with an external beam having a Gaussian intensity profile and propagating at an impact parameter (**b**), which is slightly greater than the μ-sphere radius (a). The excitation scheme can be modelled by (i) removal of the partial waves with

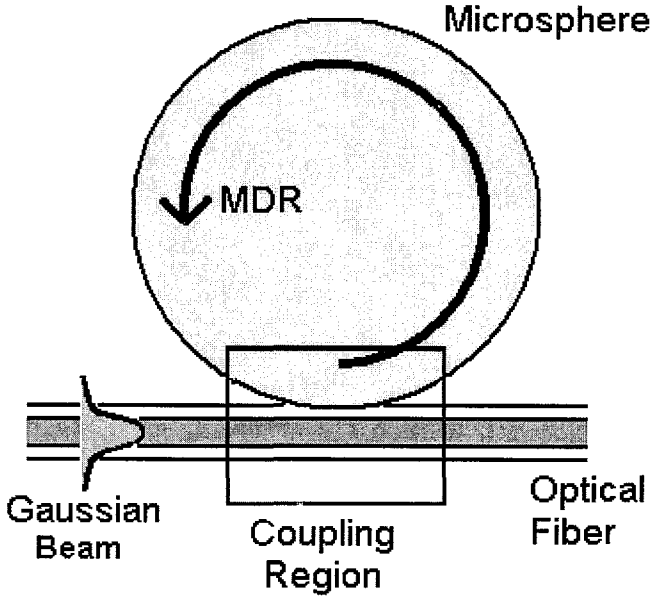

Figure 3.1 A schematic of the off- axis Gaussian beam excitation from optical fiber half coupler (OFHC).

angular-momentum quantum number n less than the size parameter ($x = 2\pi a/\lambda$) from the conventional Lorenz-Mie (plane-wave excitation) infinite series, and (ii) application of Generalized Lorenz-Mie Theory (GLMT) [21, 22] to parameterize the incident-beam profile [7, 38]. This removal of partial waves is justified by the localization principle, which associates a light ray having an impact parameter **b** with a partial wave with mode number n. This relationship can be expressed as follows [38, 33]:

$$\mathbf{b} = (n + \frac{1}{2})\frac{a}{x}. \tag{3.1}$$

Plane-wave Lorenz-Mie theory restricts the mode number (angular momentum) n range of the light rays, passing by the μ-sphere surface but yet interacting with it, to be $\mathbf{m}x \geq n \geq x$, where **m** is the relative refractive index of the μ-sphere with respect to the outside medium. This condition, together with the localization principle, restricts the impact parameter **b** range to be $\mathbf{m}a \geq \mathbf{b} \geq a$ [38]. Therefore, only the light rays within the impact parameter range of $\mathbf{m}a \geq \mathbf{b} \geq a$ can couple to the MDR's of the μ-sphere (see Fig. 3.2).

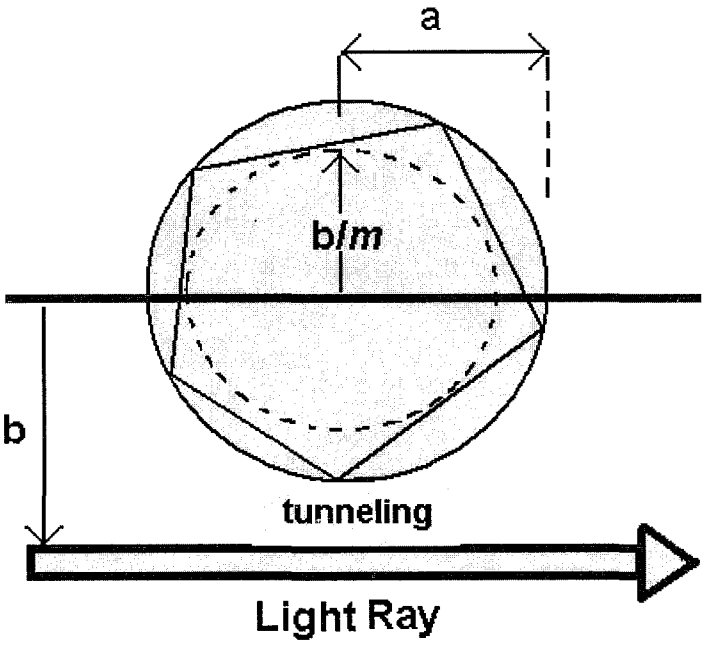

Figure 3.2 A schematic of the Localization Principle.

The coupling (scattering) efficiency can be estimated by calculation of the power coupled (scattered) into the partial-wave modes. The power coupled (scattered) into a mode can be calculated by use of the scattering cross section σ. The power coupled into a mode can be expressed as the ratio of the partial-wave scattering cross section σ_{mode} to the total cross section σ_{total} multiplied by the incident beam power P_i or, equivalently, σ_{mode} multiplied by the average incident beam intensity $< I_i >$ [38]. The power leaking (coupling out) from a mode is proportional to the energy E stored in the mode divided by the time constant τ of that mode. Hence the total power going into a mode can be expressed as [38]

$$\frac{dE}{dt} = \frac{\sigma_{mode}}{\sigma_{total}} P_i - \frac{E}{\tau} =< \sigma_{mode} > P_i - \frac{E}{\tau} = \sigma_{mode} < I_i > - \frac{E}{\tau} \tag{3.2}$$

where we have defined σ_{mode} as the scattering (or power coupling) efficiency into a mode. Then the steady-state energy E_0 in the mode can be expressed as

$$E_0 = \frac{\sigma_{mode}}{\sigma_{total}} P_i \tau =< \sigma_{mode} > P_i \tau = \sigma_{mode} < I_i > \tau \tag{3.3}$$

For a plane wave, the total cross section σ_{total} is $2\pi a^2$. A Gaussian beam with the same intensity as the plane wave, however, has a total cross section of $\pi\omega_0^2/2$, where ω_0 is the beam waist half width. Therefore, an off-axis Gaussian beam will couple more efficiently into a mode if it happens to be propagating at the impact parameter **b** corresponding to that mode [38].

3.2 Experimental Coupling Setup

The schematic of the experimental setup is shown in Fig. 3.3. Light is coupled to the μ-sphere by using an optical fiber half coupler (OFHC) (see Fig. 3.3). The

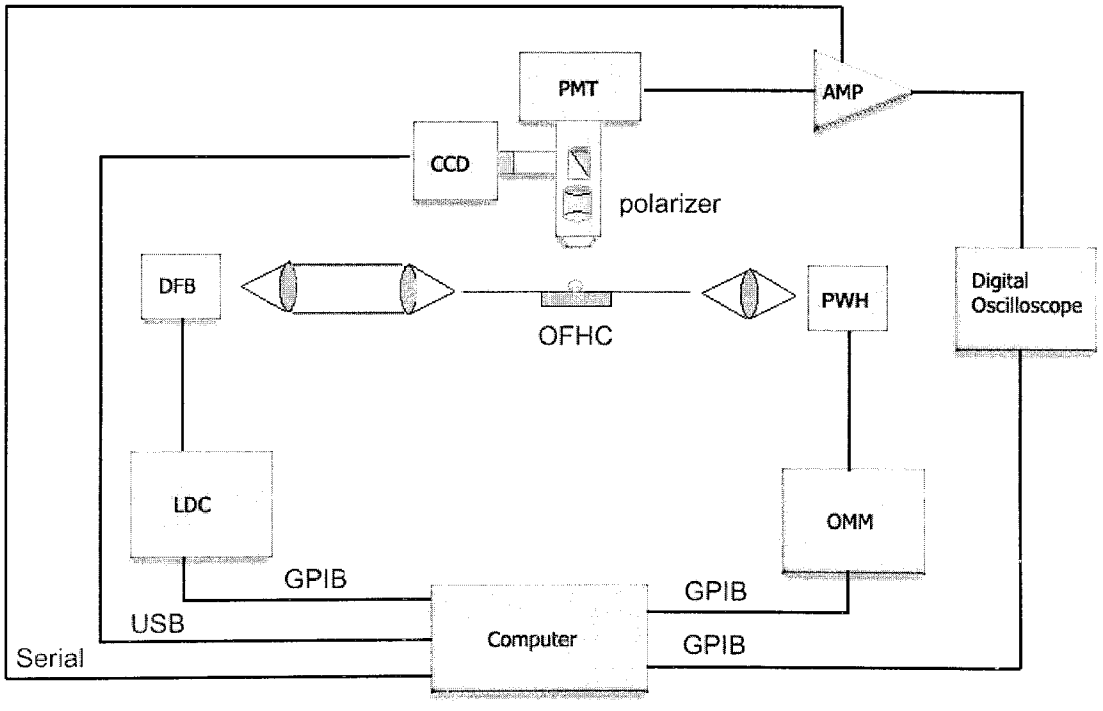

Figure 3.3 The schematic of the experimental setup.

optical fiber half coupler (OFHC) used in our experiments is fabricated from a single mode fiber, which is placed into a glass substrate. The fiber is side polished beneath the μ-sphere, until the necessary cladding thickness is achieved. Transmission loss of

the OFHC is 21 dB (i.e., 0.8%) when it is not loaded by the μ-sphere. Excitation of MDR's of the μ-sphere is achieved by using a tunable distributed feedback (DFB) semiconductor laser, whose center wavelength is 810 nm. Wavelength tuning is achieved by tuning the temperature of the DFB laser with a laser diode controller (LDC). A temperature to wavelength conversion curve is used, which is obtained by a monochromator instead of OMM, which has lower resolution than that of the monochromator (see Fig. 3.4). The abrupt change in wavelength with respect to the temperature is not seen in our measurements (The situation is attested to the mode hopping of the DFB laser). Both the transmitted light through the optical fiber, and the scattered light from the μ-sphere at right angle (90^o) are detected. A polarizer is inserted between the microscope and the photomultiplier tube (PMT) to separate the TE and the TM

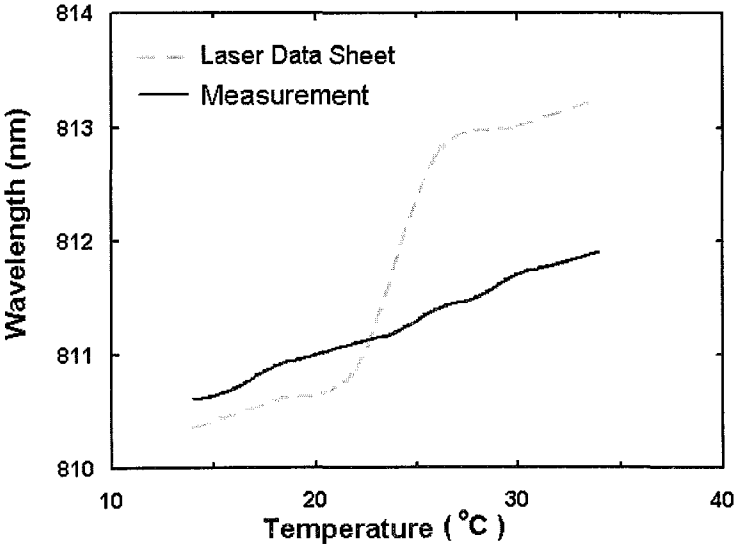

Figure 3.4 The calibration plot used for temperature to wavelength conversion.

MDR's. The PMT signal is sent to a digital oscilloscope for signal monitoring and data acquisition. The optical power and the wavelength of the transmitted light are measured by an optical multimeter (OMM) with a silicon power/wavehead (PWH). Device control and data acquisition are performed with standard IEEE-488 GPIB interface.

3.3 Data Acquisition and Control System

Since manual control and data acquisition are time consuming processes, it is beneficial to design of a software program (LDC&OMM&TDS software) to control the experimental setup. Figure 3.5 shows the user interface of the control and data acquisition software for the instrumental system. The LDC&OMM&TDS software

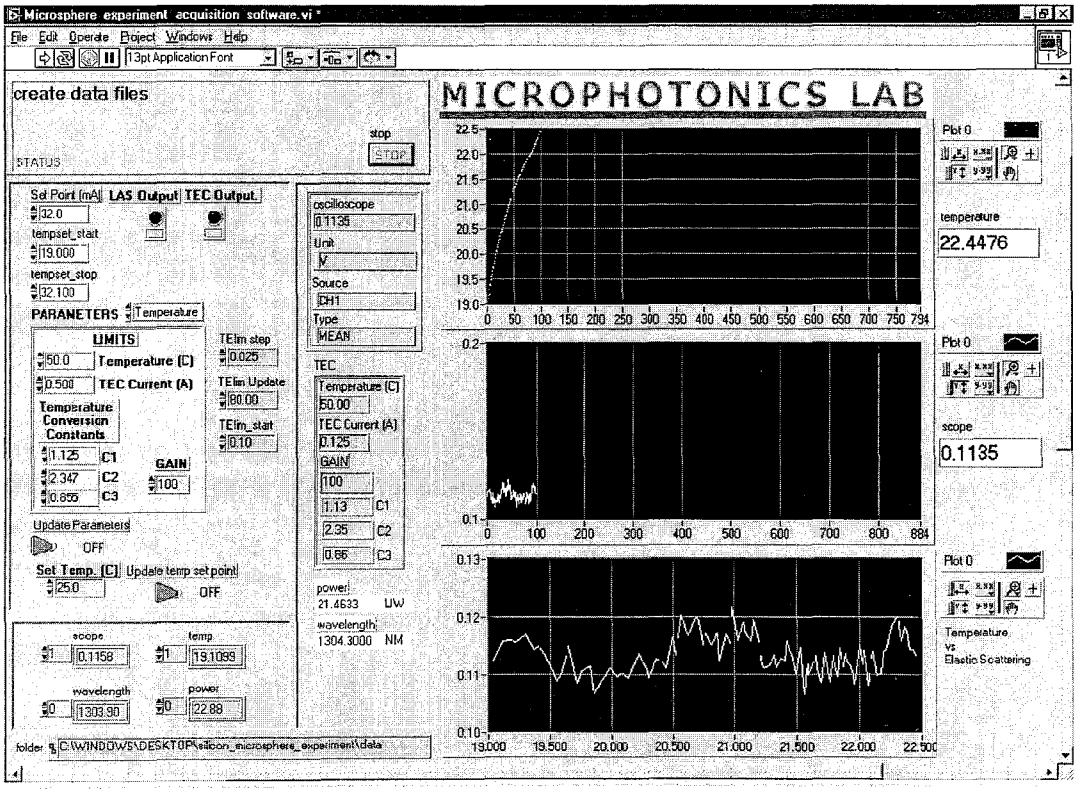

Figure 3.5 User interface of the LDC&OMM&TDS software.

provides an interface between an ILX Lightwave® LDC 3744B Laser Diode Controller, an ILX Lightwave® OMM 6810B Optical Multimeter, and a Tektronix® TDS 210 Digital Oscilloscope.

The application gets spectral data by tuning the temperature via LDC at constant current mode. The system designed upon National Instruments-VISA, which is an I/O Application Programming Interface (API) for instrumentation programming (see Appendix A). The communication along the instruments is achieved via General Purpose Interface Bus (GPIB). Our GPIB system uses a single GPIB interface to

communicate with several GPIB instruments in a linear configuration. Each instrument is configured to use a different primary address. The GPIB controller acquires and displays a fixed number of readings from each instrument. The programming is based on Single-Threaded Solution. The data acquisition and controls steps for the single-threaded solution is shown in Table 3.1.

Table 3.1
Data acquisition and control steps

Step	Operation
1	Set the control parameters for LDC TEC and LAS operations
2	Set the TDS reading to "Mean" measurement and acquisition channel
3	Initialize the OMM
4	Go to starting temperature value
5	Scan temperature up till the stop temperature point is reached
6	While more readings to acquire: Tell LDC to send data Acquire data from LDC Tell TDS to send data Acquire data from TDS Tell OMM to send data Acquire data from OMM Display acquired data
7	Save data to the specified folder

Data acquisition speed in the system is determined by the amount of the data demanded from the instruments and their response time over GPIB. This situation affects the sampling rate of the acquisition system when talk and listen to the instruments are slow since the temperature tuning is fast, which is dependent on LDC thermoelectric controller (LDC TEC). To overcome this limitation, the software interferes with Partial Integral Derivative (PID) control loop of LDC TEC and adjusts TEC current output. This method allows increase in the number of readings from the system. The user interface is mainly composed of LDC parameter controls and status displays for various settings of LDC, OMM and TDS. LDC can operate at constant power or constant current mode. In our application, Constant mode is selected as the software default. The parameters "Temperature Conversion Constants" are the sensor calibration constants

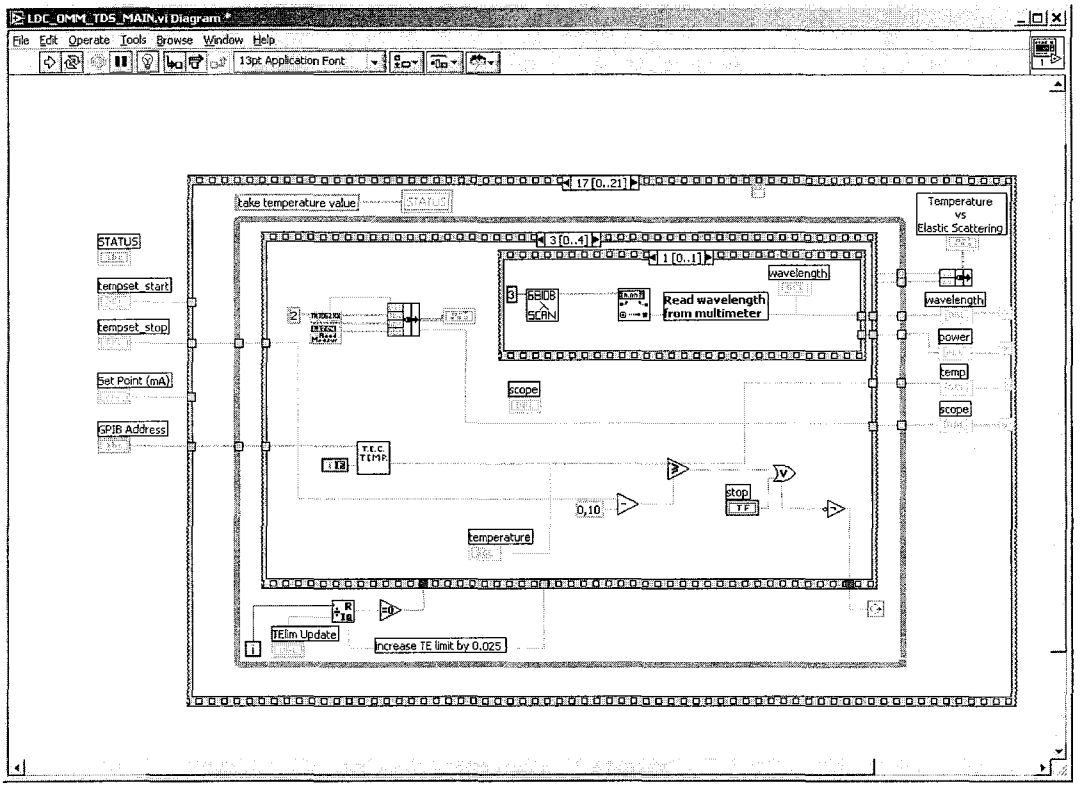

Figure 3.6 Programming diagram of the LDC&OMM&TDS software.

are necessary for accurate conversion to actual temperature. Please refer to whitepaper of your thermistor used in LDC for necesaary information. The graphs display the acquired signal from TDS, temperature from LDC and temperature vs signal.

The software was written mainly in National Instruments LabVIEW® version 5.1 for Windows. Figure 3.6 shows a snapshot of the programming diagram in LabVIEW® environment. Most of the low- level sub virtual instruments (VI) utilized were from the device manufacturers' software resources.

3.4 Experimental Results

3.4.1 Sapphire microspheres

Results of the elastic scattering experiment performed with a sapphire μ-sphere of radius 150 μm and refractive index 1.77 are presented. Fig. 3.7(a) and (b) show the experimental TE and TM elastic scattering spectra collected through a polarizer with

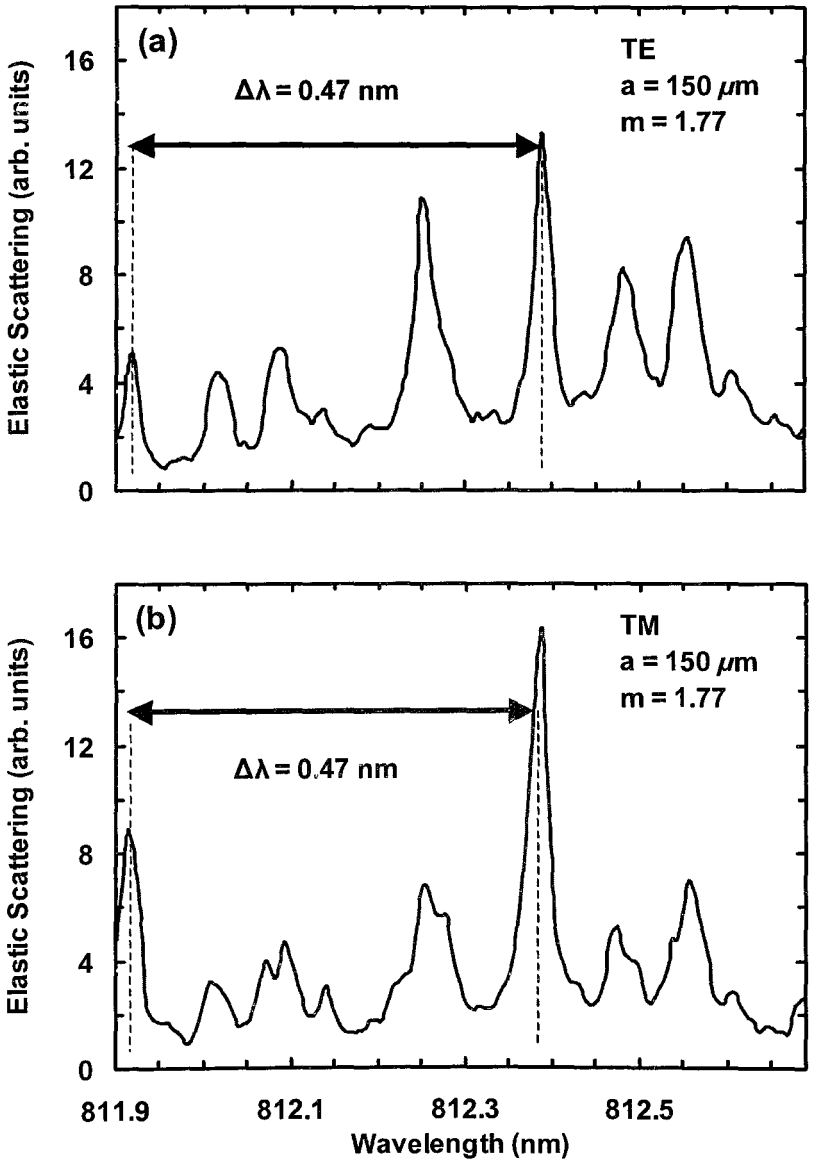

Figure 3.7 Experimental (a) TE and (b) TM elastic scattering spectra from the sapphire μ-sphere with a radius of 150 μm.

its polarization axis at 90^o to the incoming beam, and 0^o, respectively. $\Delta\lambda$ between the MDR's of the same order ℓ is 0.47 nm. Measurements indicate that Q-factors of MDR's exceed 4×10^4 (e.g., the MDR at 812.37 nm of the TE spectrum). However, scattering intensity of other MDR's are low, probably due to surface imperfections and absorption losses. Our simulation results (see Fig. 3.8) show that MDR's reach Q-factors of 4×10^5 without absorption losses. The step size used in the calculations is 0.035 nm, which is compatible with the DFB laser resolution. $\Delta\lambda$ is 0.46 nm, which is consistent with the experimentally obtained value.

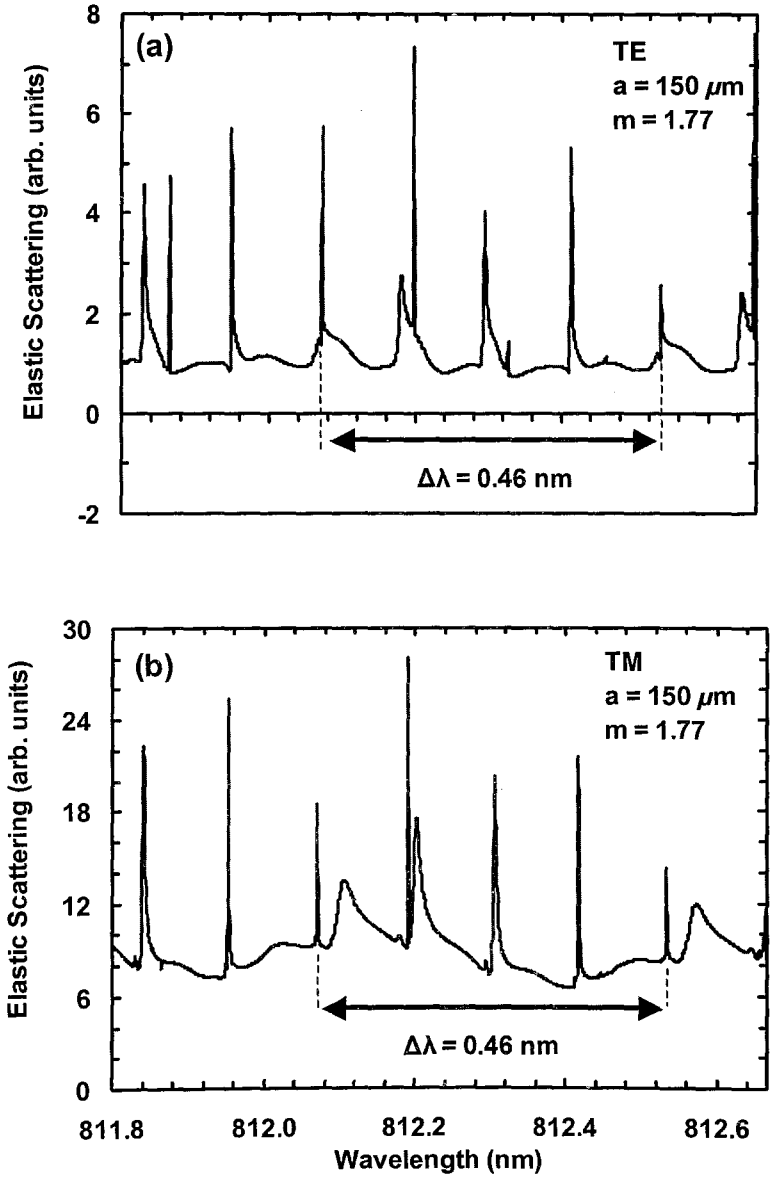

Figure 3.8 Calculation of (a) TE and (b) TM elastic scattering spectra from the sapphire μ-sphere with a radius of 150 μm.

3.4.2 Comparison of Sapphire and Glass microspheres

In Fig. 3.9(a) and (b), the mode and order numbers are calculated for both TM and TE MDR's at a wavelength range between 1530 nm and 1565 nm corresponding to C-band for a sapphire μ-sphere with the radius of $a = 30$ μm and a refractive index of $\mathbf{m} = 1.77$, respectively. The same calculations are performed for the same size ($a = 30$ μm) BK7 glass μ-sphere with a refractive index of $\mathbf{m} = 1.50$ (see Fig. 3.10(a) and (b)).

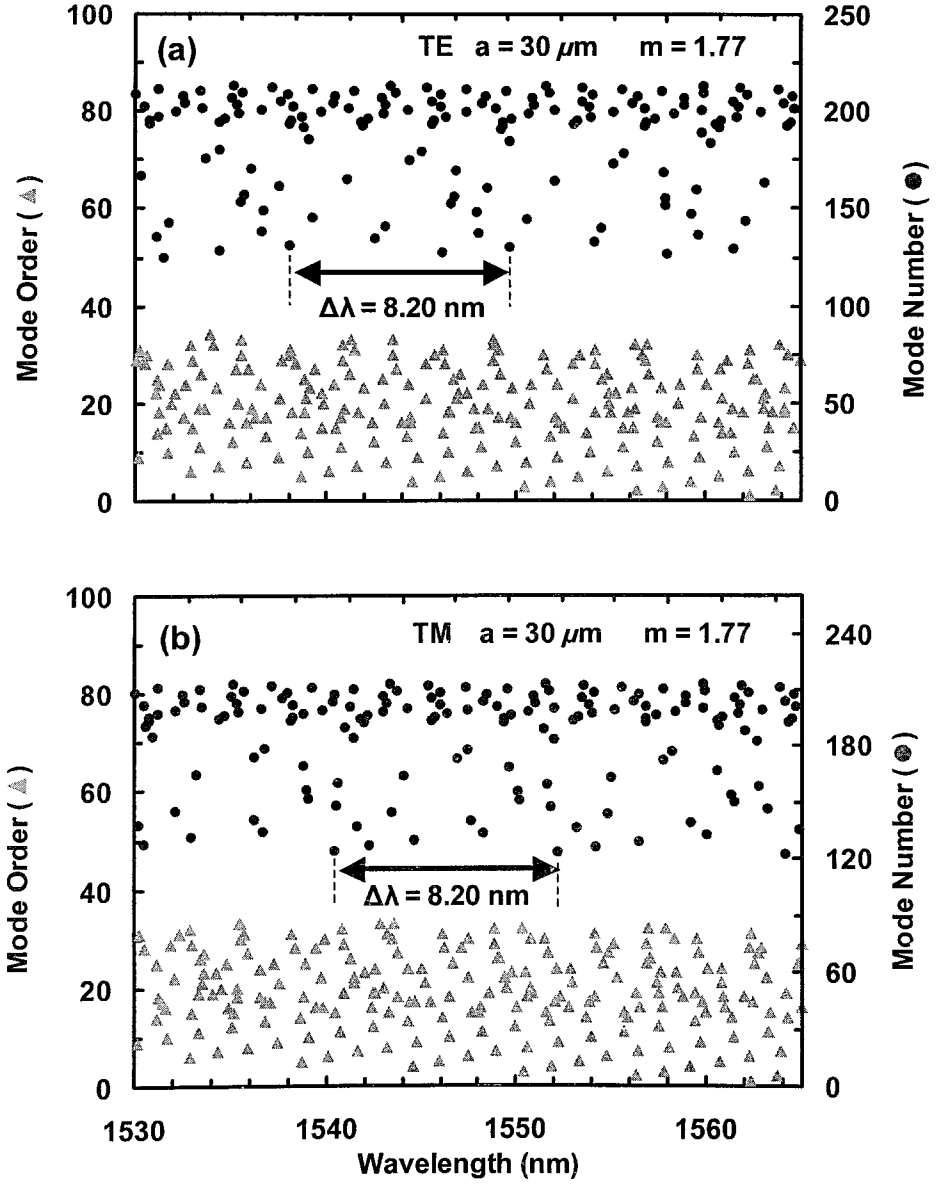

Figure 3.9 Calculated (a) TE and (b) TM mode numbers n and mode orders ℓ in elastic scattering from the sapphire μ-sphere ($a = 30$ μm, $\mathbf{m} = 1.77$) between 1530 nm and 1565 nm.

It is clearly seen in Fig. 3.9 and Fig. 3.10, that the sapphire μ-sphere possesses more MDR's than the same size glass μ-sphere, since sapphire has a higher refractive index than that of glass. Also, a large index contrast is desired at the μ-sphere - medium interface to reduce the diffraction losses for a given μ-sphere size

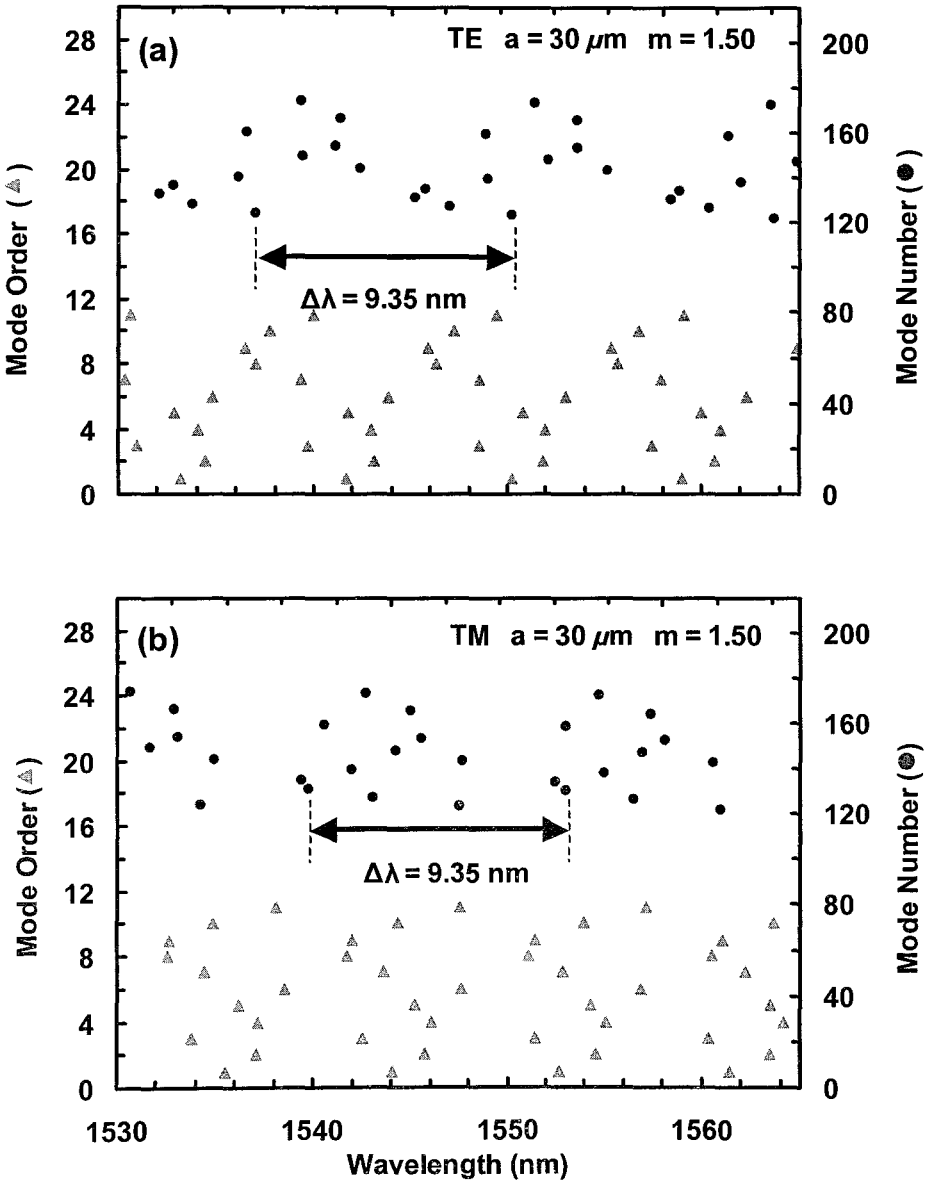

Figure 3.10 Calculated (a) TE and (b) TM mode numbers n and mode orders ℓ of the BK7 glass μ-sphere (a = 30 m, $\mathbf{m}$ = 1.50) between 1530 nm and 1565 nm.

TE and TM elastic scattering spectra for both sapphire and glass μ-spheres with a radius of 30 μm are calculated in Fig. 3.11(a) and (b), and Fig. 3.12(a) and (b), respectively. The calculated TE and TM elastic scattering spectra of sapphire

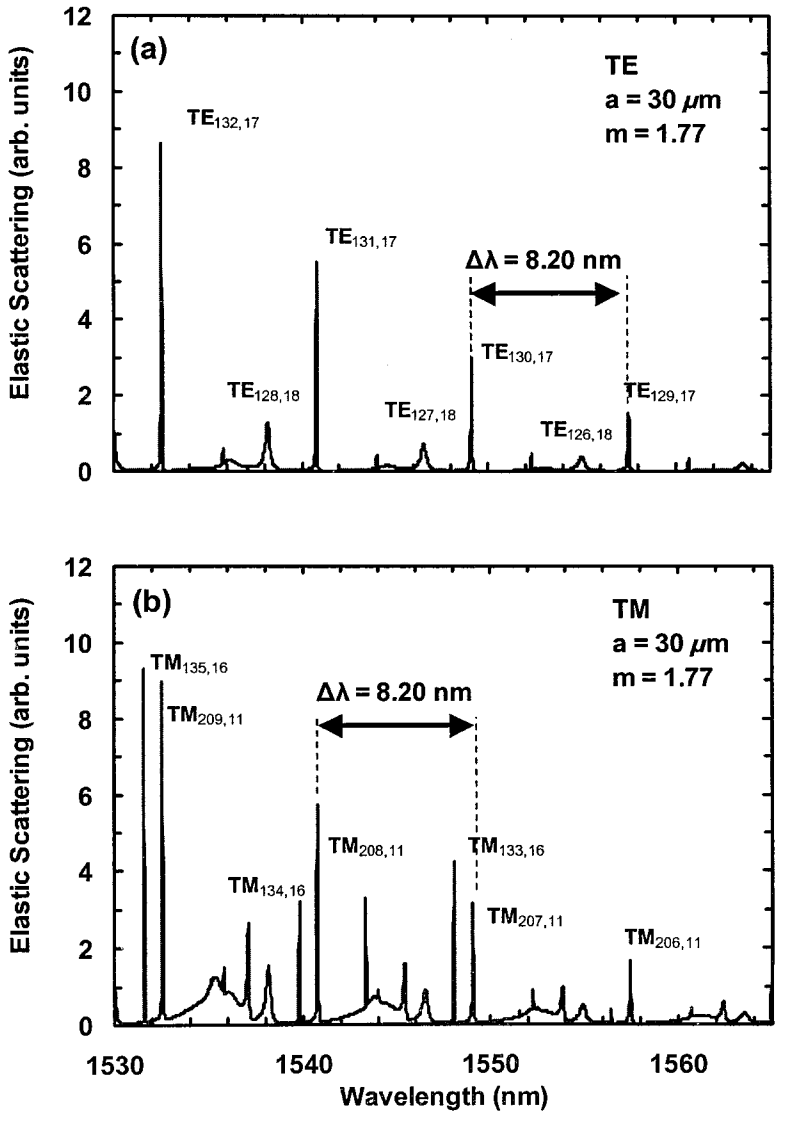

Figure 3.11 Calculated elastic scattering spectra from the sapphire μ-sphere (a = 30 m, $\mathbf{m}$ = 1.77) with both for (a) TE and (b) TM polarization.

μ-sphere (a = 30 μm) with observable MDR's respectively are shown in Fig. 3.11(a) and (b). We have also identified the mode numbers and mode orders of the MDR's. The $\Delta\lambda$ of the sapphire μ-sphere is calculated to be 8.20 nm. In Fig. 3.12(a) and (b), TE and TM elastic scattering spectra of glass μ-sphere show observable MDR's. Most of the MDR's are not observable in the spectrum due to their high Q-factors. $\Delta\lambda$ of subsequent mode orders is calculated to be 9.35 nm. Q - factors of MDR's are approximately 10^4.

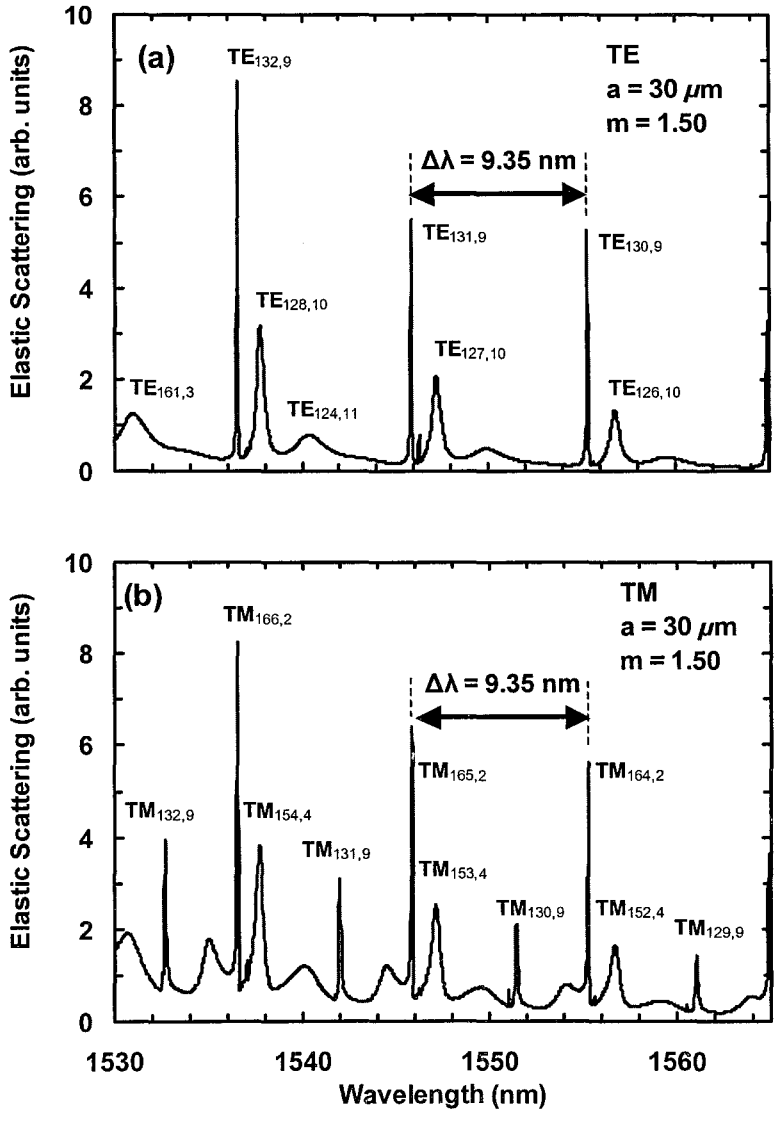

Figure 3.12 Calculated elastic scattering spectra from the glass μ-sphere (a = 30 m, $\mathbf{m}$ = 1.50) with both for (a) TE and (b) TM polariza - tion.

3.4.3 Glass microspheres

Excitation of MDR's of BK7 type glass μ-sphere, which has a radius of 500 μm, is observed. When coupling an external beam from the single-mode optical fiber, we see only one glare spot on the far side of the μ-sphere, as consistent with off-axis Gaussian beam theory (see Fig. 3.13). In resonance condition, the glare spot intensity is enhanced approximately by a factor of 2-3. The increase in glare spot intensity is solely due to the MDR's. In non-resonant conditions, the glare spot is due to the refraction of the light from the μ-sphere's rim.

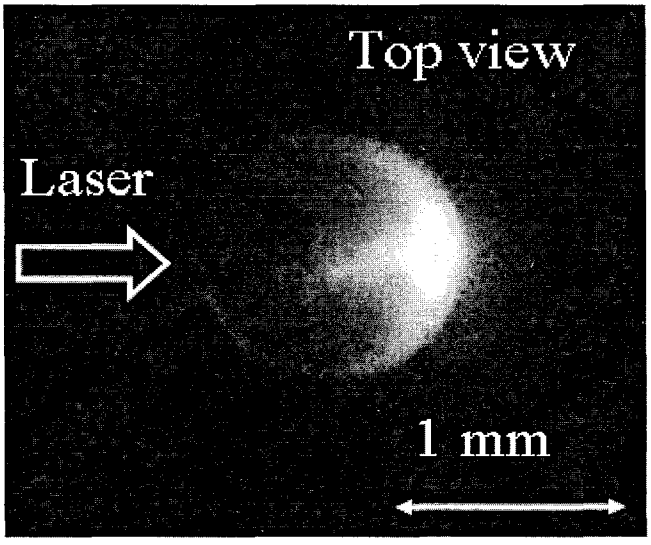

Figure 3.13 Image of the glass μ-sphere of 500 μm, when excited by the laser beam.

Fig. 3.14 shows the elastic scattering and the power transmission spectra obtained by temperature tuning of the DFB laser between 19 ^{o}C and 32 ^{o}C at a constant current of 31.2 mA. This temperature ranges corresponds to a wavelength range of 811.83 - 812.69 nm. The spectral resolution of the acquisition system is determined to be 0.004 nm. Figure 3.14(a) shows the elastic scattering spectrum of the TE MDR's, obtained through a polarizer with its polarization axis at 90^o to the incoming beam. Figure 3.14(b) is obtained, when the polarizer is placed at 0^o to the incoming beam, corresponding to TM MDR's. We can clearly observe MDR peaks in the elastic scattering, and the associated dips in the power transmission spectra. It is important to note that, the fractional depth of the dips in the transmission spectra is not the same for all MDR's. This is due to different Q-factors and coupling efficiencies of the MDR's. However, the relative depth of the transmission dips is maintained at each $\Delta\lambda$. The broad Gaussian lineshape of the power transmission spectra results from the coupling geometry of the DFB laser to the optical fiber. As the temperature of the DFB laser changes, the input laser spot moves with respect to the fiber core, when entering the OFHC.

In the spectra of Fig. 3.14, the linewidth (FWHM) of the MDR's of higher intensity is approximately 13 GHz (i.e., 0.03 nm), and the $\Delta\lambda$ of the higher intensity MDR's is measured to be 63 GHz (0.14 nm). The highest measured Q of the MDR's is

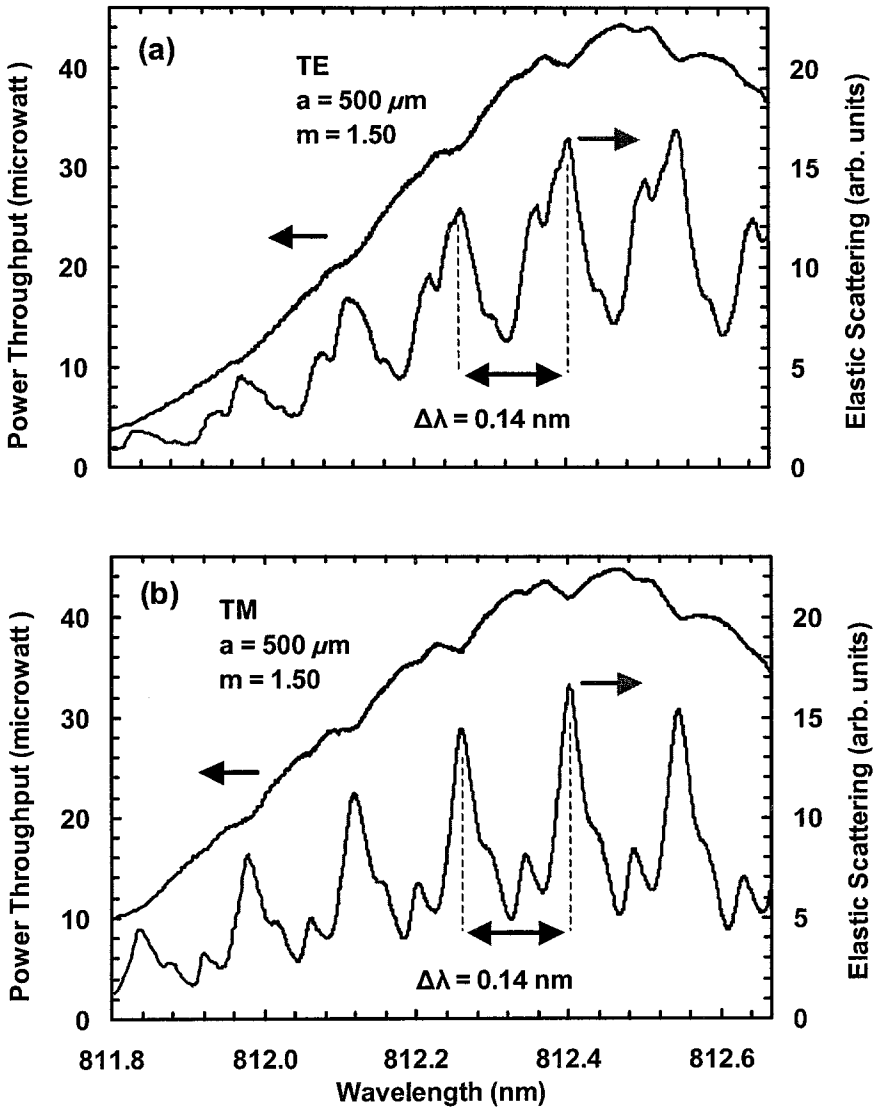

Figure 3.14 Temperature tuning spectra of the power transmission (upper curve) and the elastic scattering (lower curve) of the glass μ-sphere of 500 μm, when the polarizer is at (a) 90^o and (b) 0^o , respectively.

approximately 2×10^4. Theoretically, Q-factors of 10^9 can be reached, but these values are hard to observe [9]. In practice, absorption, scattering, and surface roughness are responsible for the measured losses corresponding to Q-factors of the order of 10^4 [12]. Furthermore, coupling efficiency is also important in excitation of the MDR's, and in observing narrow linewidth MDR's. The total quality factor (Q_T) of the MDR's for a composite fiber-μ-sphere system is defined as:

$$1/Q_T = 1/Q_0 + 1/Q_f \tag{3.4}$$

where Q_f is the Q-factor of the μ-sphere-OFHC system, and Q_0 is the intrinsic Q-factor

of the μ-sphere [38].

Power coupled into the MDR's can be estimated from the power transmission spectra. For example, in the TM spectrum of Fig. 3.14(b), the MDR at 812.4 nm has a transmitted power of 40 μW. When the μ-sphere is not present, the transmitted power is estimated to be 43 μW. Therefore, power coupled (P_i) into the MDR is approximately 3 μW, which means a 6.9 % (i.e., 0.31 dB) loss. The scattered intensity I_i can be expressed as $I_i = P_i/\sigma_{mode}$ [38]. For a Gaussian beam, the scattering cross section is defined to be $\sigma_{mode} = \omega_0\lambda/\sqrt{2}\pi$. For our experimental parameters of $\omega_0 = 2$ μm, and $\lambda = 812.4$ nm, I_i is calculated to be 0.75 kW/cm^2. We can also calculate the coupling efficiency of a Gaussian beam, $< \sigma_{mode} >$, into MDR's using the localization principle. $< \sigma_{mode} >$ is estimated to be 0.053 (i.e., 5.3%), which compares favorably with the observed 6.9% coupling loss.

3.4.4 Experiments with The Silicon Photodiode

MDR's from the 500 μm glass μ-sphere were also detected by using an unamplified silicon photodiode instead of the large PMT (see Fig. 3.15). The photodiode is

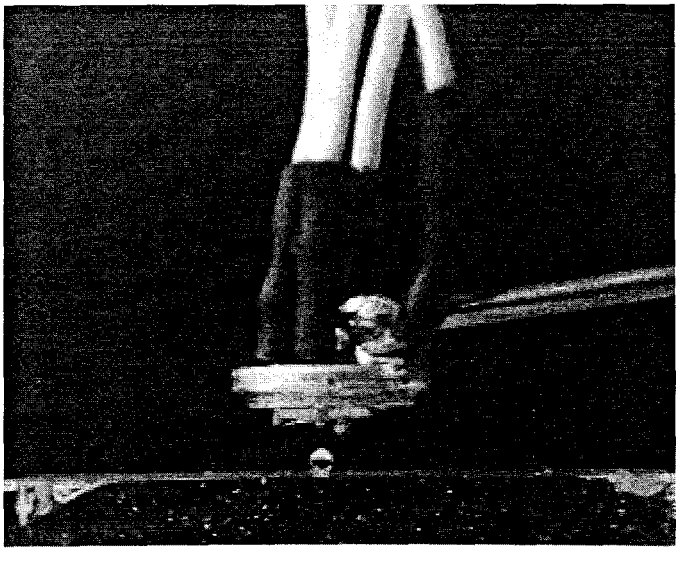

Figure 3.15 The side view picture of the optical fiber half coupler (OFHC), the μ-sphere, and the silicon detector.

placed approximately 1 mm away from the μ-sphere-OFHC system .

The elastic scattering light is collected at right angle of 90°. The signal intensity increases with the decreasing the distance of the photodiode to the μ-sphere. No polarizers were placed between the μ-sphere and the silicon photodiode. Figure 3.16 shows the experimentally obtained elastic scattering spectrum. The tuning range is between 811.32 nm and 811.83 nm. The linewidths (FWHM) of the MDR's are measured to be 0.05 nm, and $\Delta\lambda$ of MDR's is measured to be 0.14 nm. The highest measured Q of the MDR's is approximately 10^4. The Q-factors are slightly low compared to Q-

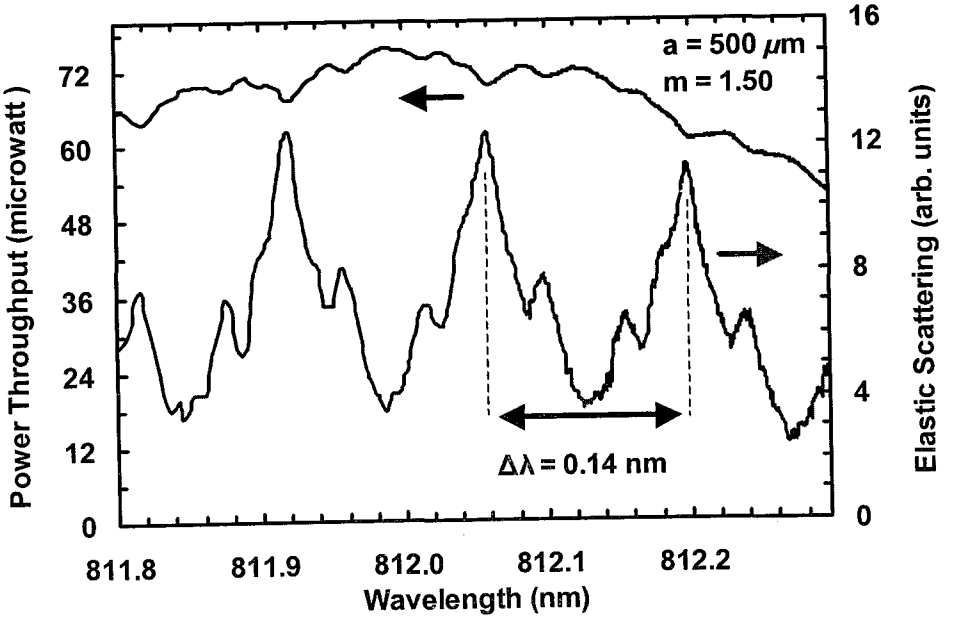

Figure 3.16 Temperature tuning spectra of the transmission (upper curve) and the elastic scattering (lower curve) spectra of the glass μ-sphere of 500 μm, obtained with the silicon photodiode.

factors of the TE and the TM MDR's spectra of Fig. 3.14. Since no polarizer is used, the spectrum gets contributions from both TE and TM modes, resulting in merged resonances.

Power coupled into the MDR's was estimated from the power transmission spectra. As an example, the MDR at 812.09 nm has a 67 μW transmitted power. When the μ-sphere is not present, the transmitted power is estimated to be approximately 75 μW. Power coupled (P_i) into the MDR is 8 μW, which means a 10.6 % (i.e., 0.49 dB)

loss in the transmission. For our experimental parameters of $\omega_0 = 2$ μm, λ=812.09 nm, the scattered intensity I_i is calculated to be 2 kW/cm^2. Coupling efficiency into MDR is estimated to be 5.3%, which compares well with the observed value of 10.6 % loss.

This OFHC, μ-sphere, and photodiode system is promising to build compact, miniaturized optical biosensor devices, which is possible with optoelectronic and microfabrication technologies.

4. BIOSENSING WITH MICROSPHERES

High Q optical μ-sphere resonators with MDR's can be used as sensitive detectors. The MDR's reside just inside the surface of the resonator, and the electromagnetic fields extend exponentially outside and die down within a few light wavelengths from the surface. A biomolecule such as a protein, that recides in the evanescent field of MDR's can absorb light, thus influencing the MDR's [5, 15, 39]. Such an influence can be detected by observing the spoiling of the Q-factor of MDR's or by observing the frequency shifts of MDR's [3, 40].

4.1 Perturbation Effects on MDR's

Perturbations due to shape deformations from sphericity, index of refraction gradients, and small inclusions all affect the resonance frequencies and linewidths of the cavity modes. Index of refraction perturbations in μ-spheres are caused by temperature gradients, composition gradients, and small inclusions, placed in and onto the μ-sphere unavoidably such as dust particles or placed deliberately such as small biomolecules.

A time-independent perturbation theory [41] was developed to calculate the effects of perturbations of dielectric microspheres on the resonant frequencies [42] and resonant widths [43].

The unperturbed system is a homogeneous sphere with permittivity $\epsilon_r = \mathbf{m}_0^2$ and radius a. The perturbed refractive index is [16]

$$\mathbf{m}(r) = \mathbf{m}_0 + \Delta\mathbf{m}(r) \tag{4.1}$$

where $\Delta\mathbf{m}(r)$ is the perturbation to the real or imaginary part of the refractive index. Ignoring terms of order $\Delta\mathbf{m}^2(r)$, the perturbation in the relative permittivity $\epsilon_l(r)$ is

given as [16] :

$$\epsilon_l(r) = \mathbf{m}^2(r) - \mathbf{m}_0^2 = 2\mathbf{m}_0\Delta\mathbf{m}(r) \tag{4.2}$$

The perturbed complex resonance size parameter x_n^0 can be expressed in terms of the unperturbed resonance size parameter x_n^{00}, using first-order perturbation theory as [16]

$$x_n^0 = x_n^{00}(1 - \frac{V}{2G}), \tag{4.3}$$

where V is the overlap of the permittivity perturbation with energy density in the mode,

$$V = \int_R dV\epsilon_l(r)[\mathbf{E}_{n,m}^+\mathbf{E}_{n,m}] = \{\frac{h_n^l(x_n^{00})}{j_n(m_0x_n^{00})}\}^2 \int_{V_s} \epsilon_l(r)|j_n(m_0k_nr)X_{n,m}|^2dV, \tag{4.4}$$

where G is the normalization integral

$$\begin{aligned} G = \lim_{R\to\infty}\int_R dV\epsilon_0(r)[\mathbf{E}_{n,m}^+\mathbf{E}_{n,m}] + \frac{i}{2\omega_n^{00}}\int_R dS\epsilon_0(R)[\mathbf{E}_{n,m}^+\mathbf{E}_{n,m}] \\ = (m_0^2 - 1)\frac{a^3}{2}[h_n^l(x_n^{00})]^2, \end{aligned} \tag{4.5}$$

and $k_n = 2\pi/\lambda_n$, λ_n is the resonance wavelength, and V_s is the volume of the μ-sphere. Recently, Arnold *et al.* has demonstrated and modelled the perturbation of MDR's by protein adsorption onto μ-spheres as a first order perturbation [5]. The method of excitation is the scheme described as the off axis Gaussian beam coupling described in the section 3.1.

When a biomolecule diffuses to the μ-sphere surface from the aqueous buffer and immobilized, it interacts with the evanescent field of MDR. This interaction polarizes the molecule and shifts the frequency of the MDR. The polarizability of a molecule describes the response of its electron cloud with the external field. The atomic or molecular energy shift ΔW due to an external electric field $\mathbf{E}$ is proportional to $\mathbf{E}^2$ for external fields which are weak compared to the internal electric fields between the nucleus and electron cloud. The electric dipole polarizability α is the constant

of proportionality defined by $\Delta W = -\alpha \mathbf{E}^2/2$. The induced electric dipole moment is $\alpha \mathbf{E}$. Technically, the polarizability is a tensor quantity but for spherically symmetric charge distributions reduces to a single number. In any case, an average polarizability is usually adequate in calculations. Polarizabilities for atoms and molecules in excited states are found to be larger than for ground states and may be positive or negative [44].

To model the shift $\delta\omega$ of MDR's in angular frequency of ω for a single biomolecule adsorbed at the surface at position a_i, it is useful to consider the energy of the interaction as a first order perturbation to a single photon resonant state, with a semiclassical field of $\mathbf{E}_0(r)exp(i\omega t)$. The evanescent tail of the field induces a dipole moment in the biomolecule in excess of the displaced water, $\delta p e^{(i\omega t)}$, causing a shift in the photon energy of the resonant state, $\hbar\delta\omega = -\delta p \cdot \mathbf{E}_0^*(r_i)/2$ as mentioned in the previous paragraph. The excess dipole moment can be represented in terms of the real part of an excess polarizability α_{ex}, i.e., $\delta p = \alpha_{ex}\mathbf{E}_0(r_i)$. The fractional frequency shift for a protein positioned at r_i is given by the result of dividing the perturbation by the energy of the mode (i.e., $\hbar\omega$), as represented by integrating over the energy density in the interior [5]:

$$(\frac{\delta\omega}{\omega})_i \cong \frac{-\alpha_{ex}|\mathbf{E}_0(r_i)^2|}{2\int \epsilon_s |\mathbf{E}_0(r)^2|} dV, \tag{4.6}$$

where ϵ_0 is the homogeneous permittivity of the μ-sphere. In case of a large number of biomolecule immobilization, singular contributions described by the Eq. 4.6 are summed up and converted into a continuous sum. As a result, the fractional frequency shift is given by a simple formula [5]:

$$\frac{\delta\omega}{\omega} \cong -\frac{\alpha_{ex}\sigma_p}{\epsilon_0(m_s^2 - m_m^2)a} \tag{4.7}$$

where σ_p is protein surface density, a is the radius of the μ-sphere, m_s and m_m are the refractive indices of the μ-sphere and the aqueous medium, respectively. The $1/a$ dependence is expected for a homogenous sphere. If such a sphere adsorbs a layer δa thick, the fractional change in frequency must preserve the condition $\delta\omega/\omega = \delta a/a$ [5].

Some of the predictions of the model proposed by Arnold *et al.* are analyzed for the case of Bovine Serum Albumin (BSA) adsorption to μ-spheres with various refractive index and size. BSA is the principal carrier of fatty acids that are otherwise insoluble in circulating plasma. The most outstanding property of albumin is its ability to bind reversibly an incredible variety of ligands. The shifts in wavelength at 1550 nm with respect to the size of the glass, polystyrene and sapphire μ-spheres are calculated The excess polarizability of BSA solution in water is $4\pi\epsilon_0(3.85\times10^{-21})\text{cm}^3$. BSA forms a compact layer of surface density, 2.7×10^{12} cm^{-2}, when BSA is in its most compact form. A surface density of 1.7×10^{12} cm^{-2} is chosen for our calculations. As seen in

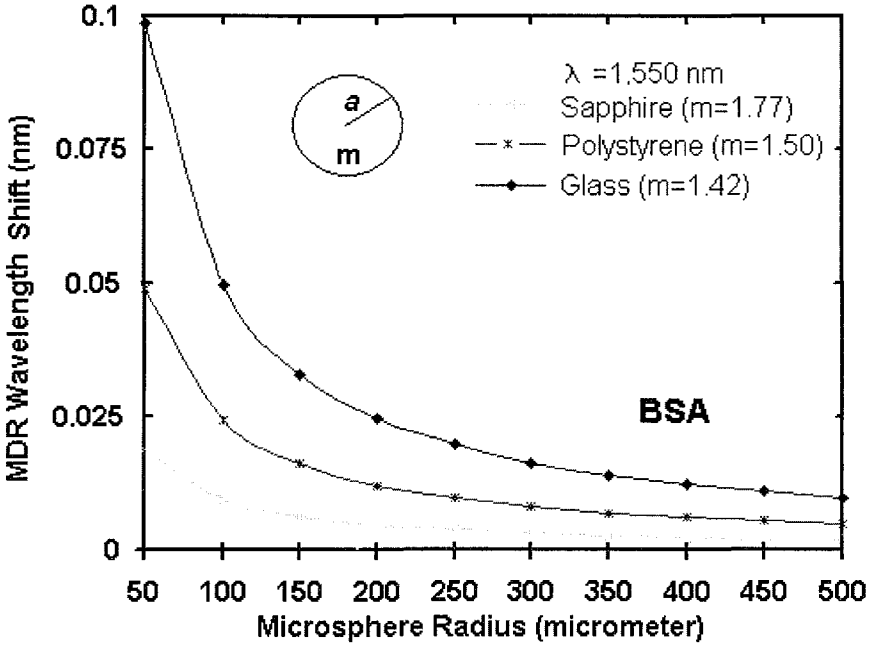

Figure 4.1 MDR wavelength shifts with respect to the radius of glass, poly- styrene, and sapphire μ-spheres.

Fig. 4.1, the MDR shifts decrease with the increasing radius for the same material type μ- spheres, which means that large μ- spheres are not so sensitive to the adsorbed BSA molecules. It is seen that increasing the refractive index causes a decrease in the resonance shifts. Sapphire, polystyrene and glass μ- spheres have refractive indices of 1.77, 1.50, 1.42, respectively. It can be concluded that, if the biosensor to detect proteins is to be built at laser light of 1550 nm, using glass μ- sphere of radius around 200-300 μm is advantageous: The MDR shifts can be measurable such as with our experimental

setup. The μ-spheres can be handled easily while the manipulation of small μ-spheres needs careful arrangements in the experimental system. Also, the tuning range of the DFB laser limits the μ-sphere size since the MDR separation decreases with the size. μ-Spheres of radius 200-300 μ posses several observable MDR's in the tuning range of the experimental system.To reach higher sensitivity, when designing a μ-sphere based biosensor, absorption of water in the buffer solution should be carefully considered. The greatest sensitivity can be obtained in $400 - 700$ nm region, around 1450 nm, and around 1940 nm for the absorption spectrum of water. 1550 nm input light is chosen for our calculations. The use of the near- IR spectral region for the design of optical μ-sphere based biosensor is quite attractive from a fabrication point of view because of the knowledge base of techniques developed by the telecommunications industry.

The capability of detecting biomolecules by MDR's of μ-spheres is not only limited with protein detection. It is also possible to monitor the hybridization reactions of oligonucleotides (oligo), fragments of single stranded DNA, for genomic assays. Adsorption of DNA to the silica μ-spheres and covalent coupling to aminosilanated glass μ-spheres are the conventional methods of immobilization as described in the previous sections. The surface capacity of immobilized oligonucleotides is in the range of 70000 molecules $/\mu m^2$ [45]. Thus depending on the strand length, the thickness of such a layer is 0.8 nm for 20-mer oligo, 1.9 nm for 50-mer oligo, and 5.8 nm for 150-mer oligo. Assuming a hybridization yield of 33 %, the increase in the thickness of added layer due to the binding of the complementary oligonucleotides is expected to be 0.3 nm for 20-mer oligo, 0.6 nm for 50-mer oligo, and 1.9 nm for 150-mer oligo.

The hybridization of long probes such as 150-mer oligos on the μ-spheres of 200-300 μ can be easily detectible in a our experimental setup, having a spectral resolution of 0.004 nm. However, the long probes may reduce hybridization efficiency by multiple attachments to the μ-sphere surface.The shifts of MDR's may be observable, if smaller μ-spheres are used. Also, with a ten times increase in spectral resolution of the the system, which can be achieved by current tuning of the DFB instead of temperature tuning, shifts of the MDR's are observable for μ-spheres of 200-300 μm. For short oligonucleotides such as 50-mer oligos, MDR wavelength shifts are shown in the Fig.

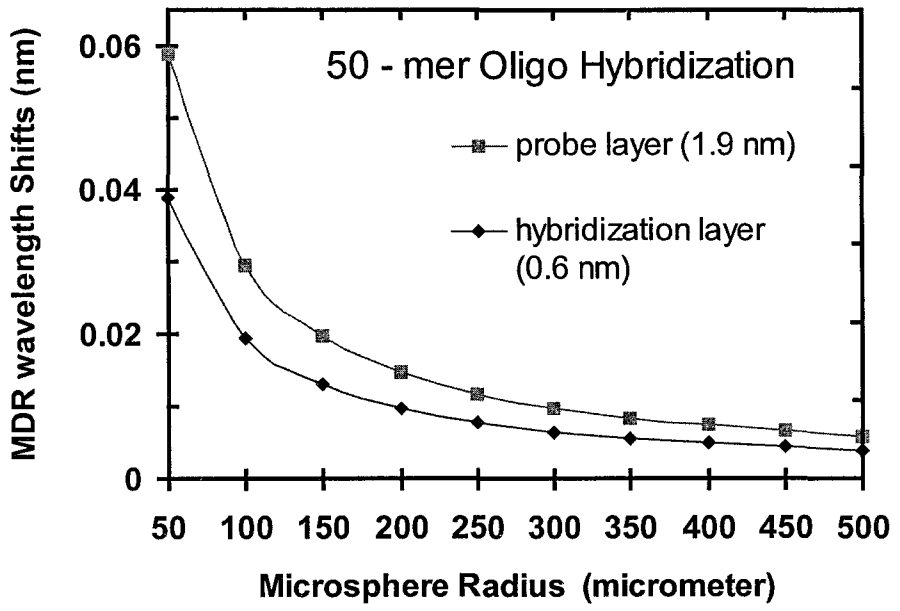

Figure 4.2 MDR wavelength shifts for hybridization of 50-mer oligos.

4.2. In practical applications, the probe layer can be immobilized covalently and the they are commercially available. Then, the attachment of the target oligos can be detected.

5. IMMOBILIZATION OF BIOMOLECULES ON MICROSPHERES

Attachment of biomolecules on solid surfaces has a key role in biosensor design, since it strongly affects the sensitivity and selectivity. Immobilization is defined as a temporary or permanent localization of biomolecules on or within a support. The biomolecule has to be properly and efficiently attached to the transducer in order to make a viable biosensor. Adsorption and covalent attachment are the regular methods of immobilization.

Many substances adsorb biomolecules on their surfaces such as glass and polystyrene. Physical adsorption is usually weak and occurs via the formation of van der Waals bonds, occasionally with hydrogen bonds or charge-transfer forces. Adsorbed biomolecule is very susceptible to changes in pH, temperature, ionic strength and the substrate. However, the method is satisfactory for short-term investigations [46].

Covalent coupling involves a carefully designed bond between a functional group in the biomolecule to the support matrix. Surface must contain reactive groups such as amines (-NH_2), carboxylic acids (-COOH), and hydroxyl groups (-OH). If the system does not have reactive surface groups, then it must first be modified. Several covalent coupling chemistries are available to immobilize the biomolecule, depending on the available reactive groups. Chemically immobilized biomolecules can also be attached via a spacer group, an "arm", "leash", or "tether". These spacer arms possess reactive end groups such as amines, carboxylic acids, and hydroxyl groups. Spacer arms can enhance steric freedom of the attached biomolecule. Multiple types of biomolecules can be attached to one supporting structure.

Techniques of Immobilization of biomolecules on solid surfaces get the driving force from genomics technologies such as DNA arrays and proteomics such as microsphere based immunoassay studies.In recent years, high-density miniaturized oligonu-

cleotide arrays have emerged as promising tools for assessing genomic data with a higher throughput than the traditional gel-based methods. Such oligonucleotide arrays, or DNA chips, have been applied to genetic mutational scanning [47], molecular bar coding [48], gene expression monitoring [49], and sequencing [50]. The development of efficient chemistries for the manufacture of spatially resolved, microscale DNA arrays on a solid-support is essential for the realization of the DNA chip technology potential. Molecules may be immobilized passively through hydrophobic or ionic interactions. However, in these cases, oligoncleotides are susceptible to removal from the surface under high salt or high temperature conditions. Covalent immobilization is often necessary for binding molecules that do not adsorb, adsorb very weakly, or adsorb with improper orientation and conformation to noncovalent surfaces. Covalent immobilization may result in better biomolecule activity, reduced nonspecific adsorption, and greater stability [51]. In developing a useful and reliable chemistry for producing DNA arrays, the accessibility and functionality of the surface-bound DNA, the density of attachment, the stability of the array, the reproducibility of the attachment chemistry, and the fidelity of the immobilized sequences are all important.

Preparation of the two dimensional array surface usually involves treatment with an amino silane reagent to the glass or silicon surface resulting in a uniform layer of primary amines or epoxides. The goal of surface modification is the maximization of performance. Surface modification provides sensitivity, maximum specificity with minimal nonspecific adsorption, and stability of the sensor surface, which increases reproducibility.

Choosing the correct surface as a solid support is a critical step in assay development. Substrates for arrays are usually silicon chips or glass microscope slides, with slides being the most common medium. Primarily due to its low fluorescence, transparency, low cost, and resistance to high temperature, glass is a popular material for DNA chip technology. Glass surfaces can be modified by silane chemistry to introduce specific functions such as amino groups, epoxide, carboxylic acid, and aldehyde. In addition, glass offers a number of practical advantages over porous membranes and gel pads. As liquids cannot penetrate the surface of the support, target nucleic acids have

direct access to the probe without internal diffusion [52]. Microscope slides are commonly used in laboratories because they are easy to handle and adaptable to automatic readers. Glass is a readily available and inexpensive support medium, possessing a relatively homogeneous chemical surface whose properties have been well studied and which is amenable to chemical modification using very versatile and well developed silanization chemistry [53].

There are a number of ways to modify solid surfaces for the covalent immobilization of biomolecules [54]. These modifications meet several criteria [55]; the linkages are chemically stable, sufficiently long to eliminate undesired steric interference from the support, and hydrophilic enough to be freely soluble in aqueous solution and not produce non-specific binding to the support [53].

Once these modifications have activated the surface, the efficiency of attaching the oligonucleotides depends largely on the chemistry used and how the oligonucleotide targets are modified. Oligonucleotides modified with an NH_2 group can be immobilized onto epoxy silane-derivatized [56] or isothiocyanate coated glass supports [53]. Succinylated oligonucleotides can be coupled to aminophenyl- or aminopropyl-derivitized glass surfaces by peptide bonds [57], and disulfide-modified oligonucleotides can be immobilized onto a mercaptosilanized glass support by a thiol/disulfide exchange reactions [58] or through chemical cross linkers.

The planar surface structure of glass slides or silicon chips can limit the loading capacity of biomolecules. Using a spherical surface, instead of planar surface, for biosensing has several advantages: The rate of biomolecule attachment onto the μ-sphere determines the response time of the sensor. A spherical shape maximizes the surface area of the sensor in contact with the sample, ultimately reducing the response time by allowing biomolecule attachment to occur in three dimensions instead of two, as occurs in traditional planar surfaces. Furthermore, spherical morphology makes the spatial orientation of the sensor within the sample unimportant. There are currently several means of attaching biomolecules to the μ-spheres used as solid supports, including adsorption to plain polymeric μ-spheres, covalent attachment to surface func-

tionalized μ-spheres, and attachment to μ-spheres that are pre-coated with a generic binding protein, such as Streptavidin.

The method of choice is relevant to the hydrophobicity of the μ-sphere's surface. Polymeric surfaces generally tend to be hydrophobic, and the original method for attachment of biomolecules to hydrophobic μ-spheres is adsorption. Covalent coupling is effective for immobilization of biomolecules to hydrophilic μ-spheres, such as silica μ-spheres.

5.1 Adsorption on Microsphere

The mechanism for adsorption is based primarily on hydrophobic attractions between the hydrophobic portions of the adsorbed biomolecule and the polymeric surface of the μ-spheres. The biomolecule of interest is attached to the μ-sphere simply by incubating the two together for a fixed amount of time. Because impurities will compete with biomolecule for space on the μ-sphere surface, both through relative affinity and relative concentration effects, maximum biomolecule adsorption requires the use of ultrapure reagents. If the concentration of an impurity is very high, it could become the principal coating. This is the means of attachment for most hydrophobic biomolecules. In the case of less hydrophobic biomolecules (or more hydrophilic μ-spheres, such as -COOH modified), attachment via both ionic interactions and hydrophobic interactions can take place. Human serum albumin and hemoglobin are examples of such biomolecules.

Adsorption of large biomolecules to hydrophobic surfaces are essentially irreversible to dilution in the same buffer used for attachment. However, adsorbed biomolecules can be displaced by competing molecules, such as proteins or surfactants. The composition of the hydrophobic polymer influences the ability of an adsorbed biomolecule to be displaced [59].

Small molecules, like haptens, will not adsorb well, or remain attached for a long

time. Covalent binding of these small molecules to proteins like Bovine Serum Albumin (BSA), or polymers such as dextran and polylysine, which will adsorb well, enhances and stabilizes their attachment to the μ-spheres. Alternatively, one could couple the hapten or other label after adsorbing the polymer or protein on the μ-spheres. Others favor a hybrid method: adsorption of phenylalanine/lysine copolymer onto polystyrene with glutaraldehyde binding of protein to the amino surface groups from the polymer [60].

It is also possible that DNA adsorbs to silica in the presence of chaotropic agents. HIV RNA is isolated from serum using NaClO4 and guanidinium thiocyanate, or guanidinium hydrochloride [61]. Now, Chaotropic-salt-induced adsorption of DNA to silica is one of the most common methods for purifying both chromosomal and plasmid DNA from cell homogenates.

5.2 Covalent Attachment on Microsphere

Covalent coupling is often employed for the immobilization of biomolecules when a very active and stable μ-sphere is required. By covalent coupling, biomolecules are permanently bound, and will not desorb /leach over time. Ligands are favorably presented on the surface of the μ-sphere, such that binding moieties are available for interaction with target molecules. Also, binding kinetics can approach those of solution-based binding [62].

Native silanol groups on the surface of silica μ-spheres are readily reacted with aqueous or solvent-based silane coupling agents to yield preactivated silica μ-spheres with a large variety of surface functional groups. Examples include chloromethyl, carboxyl, and amino groups. DNA and RNA are isolated from serum by adsorption onto silica in the presence of chaotropic agents [61]. Oligonucleotides via 5'-phosphate end can be covalently bound to amino surface-modified silica. Lipids can be bound via the -carboxyl group on the fatty acid chain and propylamine surface groups on the silica

[63]. Some evidence indicates that one can attach 10-40 % more protein covalently than by adsorption [64]. When the desired biomolecule coverage is low, covalent coupling may provide more-precise control of the coating level. The covalent bond is more thermally stable. This property could be essential if the μ-spheres are to be used in polymerase chain reaction or other applications requiring thermocycling. Hydrophilic molecules must be covalently linked to the μ-sphere surface. Unless bound to the surface, they will surely desorb when the equilibrium is disturbed by removal of unbound soluble molecules from solution. Covalent introduction of a spacer arm permits secure but flexible attachment of many different molecules. Covalent attachment of hetero- or homo- bifunctional and trifunctional cross-linkers facilitates coupling of ligands with unusual available chemical groups. Protein does not adsorb to hydrophilic silica μ-spheres; it must therefore be linked covalently to any of several coupling groups. Adsorption of DNA to μ-spheres by multiple site attachment may hinder its hybridization. The best method for attachment of DNA to μ-spheres is probably covalent coupling, at only one point of attachment, preferably at the 5', phosphate end, or 3',-OH end. DNA can be bound to either polymeric or silica μ-spheres. There are special considerations for the immobilization of single-stranded nucleic acid probes. As the full length of the oligonucleotide will participate in the hybridization event, high probe density on the bead surface has been associated with reduced hybridization efficiency due to steric effects [65]. Figure 5.1 illustrates the relationship between probe length and packing

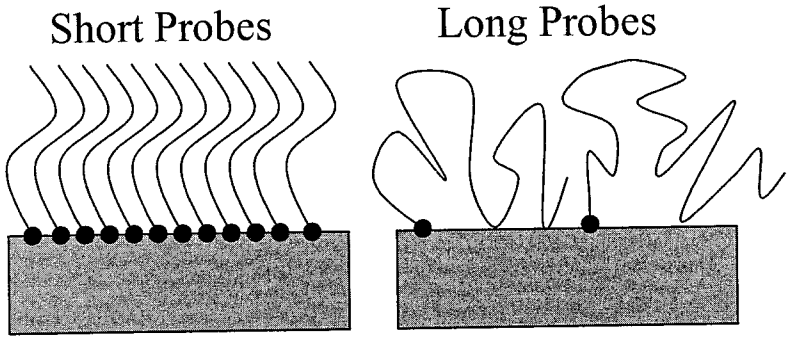

Figure 5.1 Schematic of the DNA probe length and packing configuration.

configuration / surface density: Short probes are packing in extended configurations, with long probes existing in more flexible, polymeric-like configurations.

Although the general covalent coupling protocols will typically result in some level of surface coating, it is expected that optimization will be required in order to achieve desired activity, performance, and stability. There are a number of factors and points of optimization to consider, some of which are presented in the list that follows.

Biomolecule As activity and binding kinetics are highly dependent upon orientation of the immobilized molecule, reactive groups that are available for coupling or modification should be carefully considered [66, 67].

Microsphere Biomolecules may be coupled to polymeric or silica μ-spheres through a variety of surface chemistries. Surface functional groups that are available include: polymeric - carboxyl and amino (greatest availability), as well as hydroxyl, hydrazide and chloromethyl; silica - silanol, carboxyl.

Microsphere Composition The specific composition of the μ-sphere will determine characteristics such as hydrophobicity / hydrophilicity, charge (positive / negative), surface charge density. These characteristics will have some influence on the loading capacity, i.e. how efficiently will the biomolecule come into proximity of the chemical group so that coupling may occur. They will also affect nonspecific binding characteristics, although nonspecific binding may be addressed with blockers and buffers.

Crosslinking reagent (linker, spacer, activator) There are a number of chemical compounds that may be employed to modify or bind to the available reactive group on the μ-sphere or biomolecule. Crosslinking reagents may be used to 'activate' groups that exhibit low reactivity in an aqueous environment (e.g., carbodiimide for binding to COOH groups), or to join groups that are simply not reactive toward one another (e.g., NH_2 to NH_2). Certain types of linkers function as spacers, extending the biomolecule from the solid surface (often used in the coupling of small molecules or oligonucleotides to address steric effects).

Reagent concentration Determining appropriate concentrations of different reagents such as ligand and linker will be important in controlling surface density. Using too little may result in sub-optimal coating and low activity. Use of too much

may cause μ-sphere 'overload' (steric effect, with diminished activity). Protein covalent coupling protocols [68] have historically focused on the binding of a monolayer of protein. The amount of protein that will comprise a monolayer will depend upon factors such as the molecular weight of the protein and its relative affinity for the bead.

Buffers There are a number of buffers that have been used successfully in covalent coupling reactions. Generally, the compatibility of the buffer and biomolecule (solubility, activity), and the pH at which each reaction (activation, binding, quenching, blocking) occurs will be important. The pH at which a biomolecule has a net charge of zero in a solution is known as the isoelectric point (pI) of the biomolecule. Because proteins are made up of side chains with ionizable groups, the pI of a protein is determined by its amino acid composition. The positive and negative charges on a protein exactly balance at its isoelectric point. For example, BSA has a pI of 4.7. Proteins generally have a minimum solubility when the pH of the solution is near their pI. This information to be used to maximize protein solubility or to precipitate the protein from the solution. Additionally, the buffer should not contain compounds that will interfere or compete with the reaction or ligand. For example, phosphate and acetate buffers can reduce the reactivity of carbodiimides, and are thus not recommended for use as activation buffers when coupling to -COOH modified μ-spheres. A popular alternative in this instance is MES. Also, buffers containing free amines, such as Tris or glycine, should be avoided when working with amine reactive chemistries.

Blockers Blocking agents are often coated on μ-spheres (via adsorption) following the coupling reaction. These compounds are used to minimize nonspecific interactions between the coated μ-sphere and non-target molecules in sample (e.g. hydrophobic interaction between proteins and polymer surface). The blocking agent should be selected carefully, to ensure that it is effective in minimizing nonspecific interactions; certain blockers may actually contribute to nonspecific binding. Blocker concentration should be evaluated to ensure adequate blocking (especially in light of coating level of the capture molecule), without appreciable loss of activity.

5.3 Avidin/Biotin Affinity Binding to The Microsphere

Microspheres conjugated to various types of generic binding proteins and secondary antibodies are rapidly becoming the solid support of choice in many biosensing areas, including immunological applications, nucleic acid work, and cell separation and visualization. These offer several advantages in terms of ligand attachment over traditional plain or surface-functionalized μ-spheres. Virtually any biomolecule can be biotinylated through a one step chemical reaction. These will then bind directly to streptavidin-coated μ-spheres with a bond strength approaching that of a covalent bond. In addition, because the biotinylated molecule is set off from the surface of the μ-spheres, the steric hindrance that can cause a problem when coupling to functionalized μ-spheres is reduced, especially for larger biomolecules.

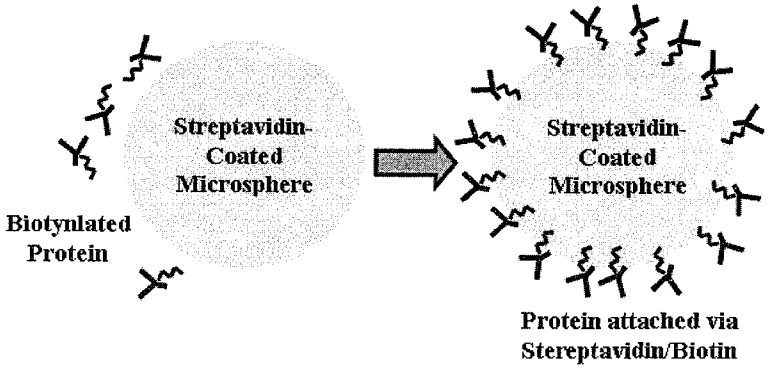

Figure 5.2 Binding of biotinylated protein to μ-sphere.

The avidin/biotin interaction is one of the strongest non-covalent bonds. This complementarity, combined with the small size of biotin, yield an ideal system for affinity binding. Avidin/biotin system does have its limitations. Avidin has carbohydrate moieties in its molecular structure, which can result in non-specific interactions with many proteins. Also, avidin's pI, the pH at which a biomolecule has a net charge of zero in a solution, of approximately 10 (a net positive charge at neutral pH), can result in non-specific interactions when working with negatively charged ligands such as nucleic acids. One solution to this is to use streptavidin, a tetrameric protein with four biotin binding sites that is similar to avidin in its molecular structure, yet lacks the

carbohydrates that can result in non-specific interactions. Streptavidin's pI of approximately 5 (a net negative charge at neutral pH) avoids non-specific charge interactions with negatively charged ligands.

5.4 Aminosilane Chemistry of Microsphere Coating

Although there are various ways of surface modification chemistry for biomolecule attachment as described in the previous sections, an easy method to coat glass surfaces is to use amionosilane chemistry, which does not require complicated laboratory equipment. To illustrate, we coated glass lamellas with gamma-aminopropyltriethoxysilane from aqueous solution to create a linker system on glass surface for biomolecule immobilization. Using glass lamellas is just to ease the test of coating. Contact Angle Measurement Test was used to reveal the coating. The chemistry is the same for glass μ-spheres. The procedure of aminosilane coating is seen in Table 5.1. This procedure

Table 5.1
The procedure of aminosilane coating

Step	Procedure
1	Prior to coating with the linker, the substrates were cleaned
2	Glass samples were placed in a 5 weight percent solution of sodium hydroxide (NaOH) for 4 minutes.
3	They were rinsed five times with distilled water
4	3 weight percent gamma-aminopropyltriethoxysilane solution is mixed with acetic acid to drop the pH of the solution to 5.5, and stirred 10 minutes
5	Glass samples are soaked in the prepared solution, and stirred 10 minutes
6	Samples were again rinsed in distilled water
7	Lamellas are finally dried for 3 hours at 120 ^{o}C

binds the aminosilane to the glass surface with functional amine groups extending outside (see Fig. 5.3).

Contact angles offer an easy-to-measure indication of the chemical bonding of the uppermost surface layers of a solid. This bonding determines wettability and

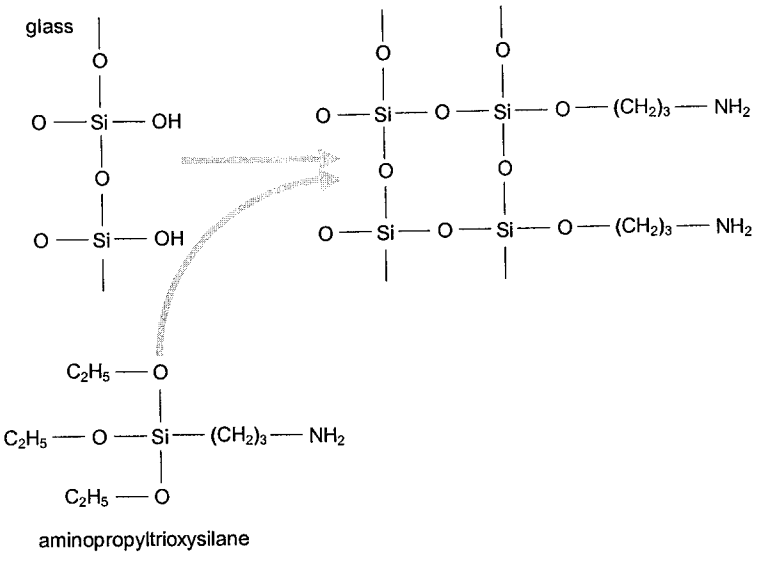

Figure 5.3 Surface modification of glass surface with gamma - aminopropyltriethoxysilane.

adhesion, and also allows prediction of coating properties and detection of trace surface contaminants.

When a drop of liquid is placed on the surface, according to the wettability of the liquid in relationship to this solid, the drop will make a certain angle of contact with the solid. The contact angle and the forces acting on the droplet are shown in Fig. 5.4. When the angle is less than 90^0, the surface is called hydrophilic. An angle greater than 90^0 signs a hydrophobic (water repellent) surface. For a plain glass surface, the contact angle for a liquid droplet is around 60^0.

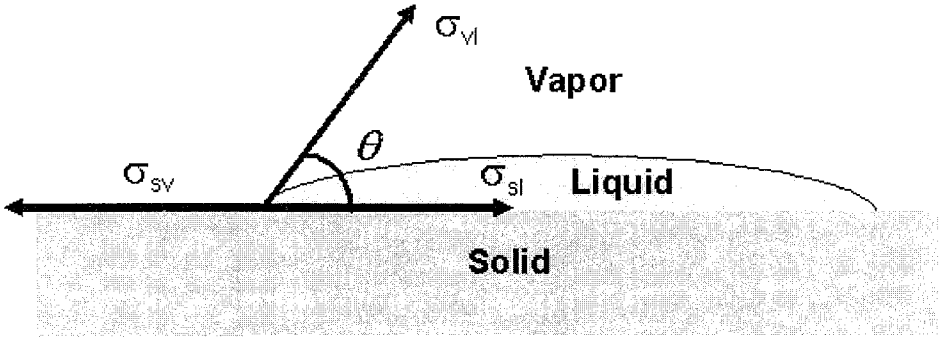

Figure 5.4 Schematic of the contact angle θ and the forces acting on the surface.

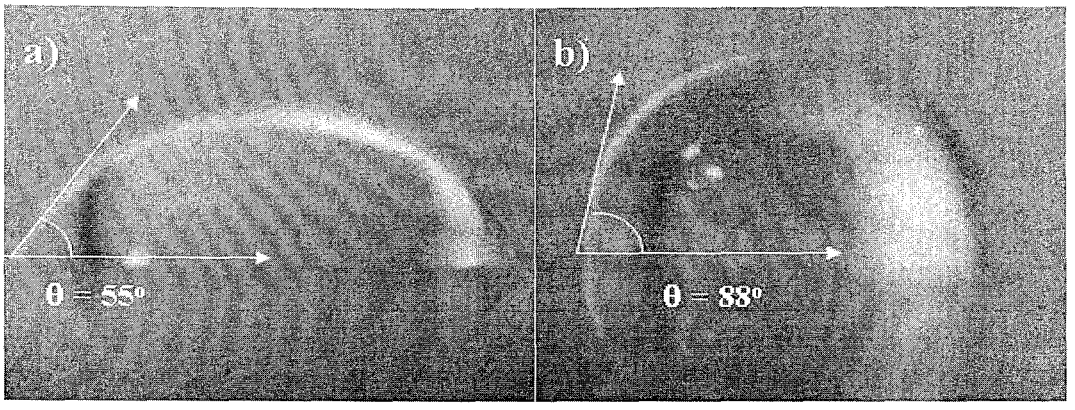

Figure 5.5 The images of water droplets and their corresponding contact angles with the (a) uncoated, and (b) coated glass surfaces.

We have measured the contact angle for both the coated lamellas and the plain lamellas, which are from the same set. The images of water droplets and their corresponding contact angles with the uncoated and coated glass surfaces are shown in Fig. 5.5. The images of water droplets on the surface of lamellas are taken with a CCD camera. Contact angle of water on plain glass surface are measured to be around 55-60^o, consistent with the values accepted. The coated glass surfaces resulted in $85-90^o$, which shows that there is coating on the glass surface, which changes the surface energy. The contact angle is directly related to the surface energy, and the important part for knowing the surface energy for various materials is mainly in material design and material selection. If the surface energy of solid is greater than the surface energy of liquid, the liquid will remain in drop shape and easy to slide out form the solid surface. Otherwise, if the surface energy for liquid is larger than the solid, the liquid will spread out above the solid surface.

6. CONCLUSIONS

Biological sensing has been an intensely active area of research, such as applications in environmental sensing, immunological studies, and genomic studies. Also, there is great need for highly sensitive techniques for the detection of trace amount of biological pathogens. In the laboratory, standard spectroscopic techniques can be used to detect various biological materials with great sensitivity and specificity, for use outside of laboratory environment, there is great need for robust, integrated devices. Integrated optics allow monitoring biological interactions in a compact geometry.

In this work, use of dielectric microspheres and their optical morphology dependent resonances to construct high sensitivity biosensors is analyzed. The excitation of MDR's of sapphire and glass μ-spheres using an optical fiber half coupler (OFCH) and, a temperature tunable distributed feedback (DFB) laser is demonstrated. Efficient coupling to MDR's is achieved with the optical fiber half coupler.

Results of the elastic scattering experiment performed with a sapphire μ-sphere of radius 150 μm and refractive index 1.77 are presented. MDR peaks in the elastic scattering spectra and associated dips in the transmission spectra are observed experimentally. $\Delta\lambda$ between the MDR's of the same order ℓ is measured to be 0.47 nm. Measurements indicate that Q-factors of MDR's exceed 4×10^4. Additionally, numerical calculations are done to compare with the experimental results. It shows that MDR's reach Q-factors of 4×10^5, without absorption losses. However, experimentally obtained scattering intensities of MDR's are relatively low, probably due to surface imperfections and absorption losses. Calculated $\Delta\lambda$ is 0.46 nm, which is consistent with the experimentally obtained value.

To further demonstrate the properties of MDR's, elastic scattering spectra from the sapphire (a = 30 m, $\mathbf{m}$ = 1.77) and glass μ-spheres (a = 30 m, $\mathbf{m}$ = 1.55) with both for TE and TM polarization are calculated. It is clearly seen that the sapphire

μ-sphere possesses more MDR's than the same size glass μ-sphere, since sapphire has a higher refractive index than that of glass.

Excitation of MDR's of BK7 type glass μ-sphere, which has a radius of 500 μm, is observed. Additionally, optical power transmission spectra are obtained. The linewidth (FWHM) of the MDR's of higher intensity is approximately 13 GHz (i.e., 0.03 nm), and the $\Delta\lambda$ of the higher intensity MDR's is measured to be 63 GHz (0.14 nm). The highest measured Q of the MDR's is approximately 2×10^4. Power coupled (P_i) into the MDR is approximately 3 μW, which means a 6.9 % (i.e., 0.31 dB) loss. The coupling efficiency of a Gaussian beam into MDR's, using the localization principle, is estimated to be 0.053 (i.e., 5.3%), which compares favorably well with the observed 6.9% coupling loss.

Detection of the MDR's of glass microsphere with an unamplified silicon photodiode in proximity to the μ-sphere is demonstrated. The linewidths (FWHM) of the MDR's are measured to be 0.05 nm, and $\Delta\lambda$ of MDR's is measured to be 0.14 nm. The highest measured Q of the MDR's is approximately 10^4. The Q-factors are slightly low compared to Q-factors of the TE and the TM MDR's spectra of the same glass microsphere with PMT detector. Since no polarizer is used, the spectrum gets contributions from both TE and TM modes, resulting in merged resonances. Coupling efficiency into MDR is estimated to be 5.3%, which compares well with the observed value of 10.6 % loss. This OFHC, μ-sphere, and photodiode geometry largely shrinks the system size, promising to build compact, miniaturized optical biosensor devices.

The MDR's of μ-spheres for biosensor applications, such as detection of proteins and DNA hybridization are described. It is seen that large biomolecules such as BSA can be detectible if the μ-sphere surface can be modified chemically. For DNA hybridization, high spectral resolution of the system is needed. Also, the chemical modification of glass surfaces by aminosilane coupling to produce functionalized μ-spheres is demonstrated. In conclusion, very sensitive biosensors based on μ-spheres working with the optical principles of MDR's can be realized and manufactured by optoelectronic and micromachining technologies.

6.1 Proposal for Future Studies

The next phase for this research may experimentally show the expected MDR shifts for various biomolecules. From this work, it was unclosed that observation of MDR shifts for glass μ-spheres of radius 200 μm for the detection of BSA molecules is feasible. In the present experimental setup, the tuning resolution should be increased for monitoring small MDR shifts such as for DNA hybridization. This can be achieved by current tuning the DFB laser. Also, after an efficient coupling into MDR's, dips in the transmission spectra can be monitored much easier than the peaks in the scattering spectra, because of the higher signal intensity. One direction in this research may be to utilize μ-spheres and MDR's for the single molecule detection. Use of visible spectral wavelengths, which probably increase the sensitivity of the biosensor because of the low absorbtion of water and of very small μ-spheres can be used to achieve this aim. A narrow linewidth Vertical Cavity Surface Emitting Laser (VCSEL) at a visible wavelength is favorable. Besides these considerations, functionalization of μ-sphere surfaces and use of specific linker molecules are necessary to specifically select and immobilize the biomolecules to be detected.

APPENDIX A. COMPUTER INTERFACING

A.1 General Purpose Interface Bus

Often referred to as the IEEE-488.2 bus, GPIB bus or HP-IB bus, the GPIB (General Purpose Interface Bus) is a standard for instrumentation communication and control for instruments from manufactures the world over. In 1965, Hewlett-Packard designed the Hewlett-Packard Interface Bus (HP-IB) to connect their line of programmable instruments to their computers. Because of its high transfer rates (nominally 1 Mbytes/s), this interface bus quickly gained popularity. It was later accepted as IEEE Standard 488-1975, and has evolved to ANSI/IEEE Standard 488.1-1987. Today, the name General Purpose Interface Bus (GPIB) is more widely used than HP-IB. ANSI/IEEE 488.2-1987 strengthened the original standard by defining precisely how controllers and instruments communicate. Standard Commands for Programmable Instruments (SCPI) took the command structures defined in IEEE 488.2 and created a single, comprehensive programming command set that is used with any SCPI instrument. The GPIB provides handshaking and interface communications over an 8 bit data bus employing 5 control and 3 handshake signals.

Equipped with a PCI-GPIB, a personal computer can:

- Control GPIB instruments
- Gather data from GPIB test equipment
- Become a data acquisition station in a GPIB system

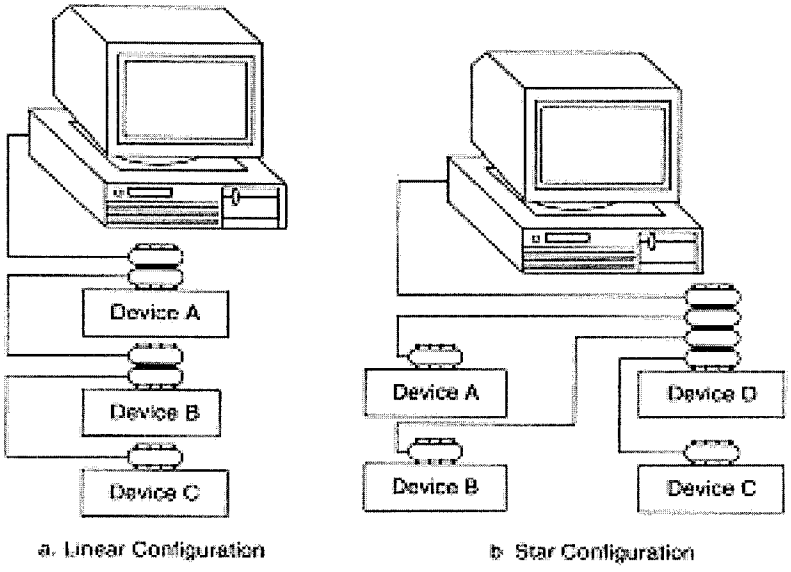

Figure A.1 General Purpose Interface Bus (GPIB) interfacing.

A.1.1 National Instrument VISA

VISA is a standard I/O Application Programming Interface (API) for instrumentation programming although VISA by itself does not provide instrumentation programming capability. VISA is a high-level API that calls into lower level drivers. The hierarchy of National Instruments-VISA is shown in the figure below.

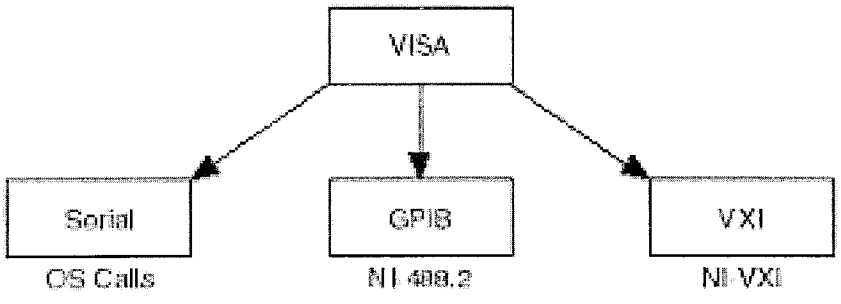

Figure A.2 The hierarchy of National Instruments-VISA.

VISA can control VXI, GPIB, or serial instruments, making the appropriate driver calls depending on the type of instrument being used. It is also possible to use one API to control a suite of instruments of different types, including VXI, GPIB

and serial. When debugging VISA problems it is important to keep in mind that this hierarchy exists. VISA uses the same operations to communicate with instruments regardless of the interface type. For example, the VISA command to write an ASCII string to a message-based instrument is the same whether the instrument is serial, GPIB, or VXI. Thus VISA provides interface independence. This makes it easier to switch bus interfaces, which means that users who must program instruments for different interfaces only need to learn one API.

VISA is designed so that programs written using VISA function calls are easily portable from one platform to another. To ensure platform independence, VISA strictly defines its own data types. Therefore issues like the size, in bytes, of an integer variable from one platform to another should not affect a VISA program. The VISA function calls and their associated parameters are uniform across all platforms. Software can be ported to other platforms and then recompiled. A LabVIEW® program can be ported to any platform supporting LabVIEW®.

REFERENCES

1. Bronzino, J., *The Biomedical Engineering Handbook*, Boca Raton: CRC Press, 2000.

2. Ilchenko, V. S., P. S. Volikov, V. L. Velichansky, F. Treussart, V. Lefervre-Seguin, J. M. Raimond, and S. Haroche, "Strain-tunable high-q optical microsphere resonator," *Optics Communications*, Vol. 145, pp. 86–90, 1998.

3. Arnold, S., "Microspheres, photonic atoms and the physics of nothing," *American Scientist*, Vol. 89, pp. 414–421, 2001.

4. Vollmer, F., D. Braun, A. Libchaber, M. Khoshsima, I. Teraoka, and S. Arnold, "Protein detection by optical shift of a resonant microcavity," *Aplied Physics Letters*, Vol. 80, no. 21, pp. 4057–4059, 2002.

5. Arnold, S., M. Khoshima, I. Teraoka, S. Holler, and F. Vollmer, "Shift of whispering-gallery modes in microspheres by protein adsorption," *Optics Letters*, Vol. 28, no. 4, pp. 272–274, 2003.

6. Collot, L., V. Lefevre-Seguin, M. Brune, J. M. Raimond, and S. Haroche, "Very high q whispering-gallery mode resonances observed on fused silica microspheres," *Europhys. Lett.*, Vol. 23, pp. 327–334, 1993.

7. Serpengüzel, A., S. Arnold, and G. Griffel, "Excitation of resonances of microspheres on an optical fiber," *Opt. Lett.*, Vol. 20, no. 7, pp. 654–656, 1995.

8. Lefevre-Seguin, V., "Whispering-gallery mode lasers with doped silica microspheres," *Optical Materials*, Vol. 11, no. 2-3, pp. 153–165, 1999.

9. Lefevre-Seguin, V., and S. Haroche, "Towards cavity-qed experiments with silica microspheres," *Materials Science and Engineering B*, Vol. 48, no. 1-2, pp. 53–58, 1997.

10. Kuwata-Gonokami, M., and K. Takeda, "Polymer whispering gallery mode lasers," *Optical Materials*, Vol. 9, no. 1-4, pp. 12–17, 1998.

11. Spillane, S. M., T. J. Kippenberg, and K. J. Vahala, "Ultralow-threshold raman laser using a spherical dielectric microcavity," *Nature*, Vol. 415, no. 6872, pp. 621–623, 2002.

12. Ilchenko, V. S., P. S. Volikov, V. L. Velichansky, F. Treussart, V. Lefevre-Seguin, J. M. Raimond, and S. Haroche, "Strain-tunable high-q optical microsphere resonator," *Optics Communications*, Vol. 145, no. 1-6, pp. 86–90, 1998.

13. Cai, M., G. Hunziker, and K. J. Vahala, "Fiber-optic add-drop device based on a silica microsphere-whispering gallery mode system," *IEEE Photon.Technol. Lett.*, Vol. 6, no. 6, pp. 686–687, 1999.

14. Tapalian, H. C., J. P. Laine, and P. A. Lane, "Thermooptical switches using coated microsphere resonators," *IEEE Photon.Technol. Lett.*, Vol. 14, no. 8, pp. 1118–1120, 2002.

15. Boyd, R. W., and J. E. Heebner, "Sensitive disk resonator photonic biosensor," *Applied Physics*, Vol. 40, no. 31, pp. 5742–5747, 2001.

16. Wolf, E., *Progress In Optics*, Elsevier, Netherlands, 2000.

17. Sandoghdar, V., F. T. F, J. Hare, V. Lefevre-Seguin, J. M. Raimond, and S. Haroche, "Very low threshold whispering-gallery-mode microsphere laser," *Physical Review A*, Vol. 54, no. 3, pp. 1777–1780, 1996.

18. Serpengüzel, A., S. Küçükşenel, and R. K. Chang, "Microdroplet identification and size measurement in sprays with lasing images," *Optics Express*, Vol. 10, no. 3, pp. 118–1132, 2002.

19. Nussenzveig, H. M., *Diffraction Effects in Semiclassical Scattering*, Cambridge University Press, Cambridge, 1992.

20. Griffel, G., S. Arnold, D. Taskent, A. Serpengüzel, J. Connolly, and N. Morris, "Morphology dependent resonances of a microsphere, optical fiber system," *Opt. Lett.*, Vol. 25, no. 10, pp. 695–697, 1996.

21. Lock, J. A., and G. Gouesbet, "Rigorous justification of the localized approximation to the beam shape coefficients in generalized lorenz-mie theory. i. on-axis beams," *J. Opt. Soc. Am. A*, Vol. 11, no. 9, pp. 2503–2515, 1994.

22. Gouesbet, G., and J. A. Lock, "Rigorous justification of the localized approximation to the beam shape coefficients in generalized lorenz-mie theory. ii. off-axis beams," *J. Opt. Soc. Am. A*, Vol. 11, no. 9, pp. 2516–2525, 1994.

23. Barber, P. W., and R. K. Chang, *Optical Effects Associated with Small Particles*, World Scientific, Singapore, 1998.

24. Benner, R. E., P. W. Barber, J. F. Owen, and R. K. Chang, "Observation of structure resonances in the fluorescense spectra from microspheres," *Phys. Rev. Lett*, Vol. 44, pp. 475–478, 1980.

25. van de Hulst, H. C., *Light Scattering by Small Particles*, Dover, New York, 1981.

26. Conwell, P. R., P. W. Barber, and C. K. Rushforth, "Resonant spectra of dielectric spheres," *J. Opt. Soc. Am. A*, Vol. 1, no. 1, pp. 62–66, 1984.

27. Schiller, S., and R. L. Byer, "High-resolution spectroscopy of whispering gallery modes in large dielectric spheres," *Opt. Lett.*, Vol. 16, no. 15, p. 1138, 1991.

28. Lam, C. C., P. T. Leung, and K. Young, "Explicit asymptotic formulas for the positions, widths, and strengths of resonances in mie scattering," *J. Opt. Soc. Am. B*, Vol. 9, no. 9, pp. 1585–1592, 1992.

29. Chylek, P., "Resonance structure of mie scattering: distance between resonances," *J. Opt. Soc. Am. A*, Vol. 7, no. 9, p. 1609, 1990.

30. Hill, S. C., and R. E. Benner, "Morphology-dependent resoances associated with stimulated processes in microspheres," *J. Opt. Soc. Am. B*, Vol. 3, no. 11, pp. 1509–1514, 1986.

31. Barton, J. P., D. R. Alexander, and S. A. Schaub, "Internal fields of a spherical particle illimunated by a tightly focused laser beam: Focal point positioning effects at resonance," *J. Appl. Phys*, Vol. 65, no. 8, pp. 2900–2906, 1989.

32. Gouesbet, G., B. Maheu, and G. Grehan, "Light scattering from a sphere arbitrarily located in a gaussian beam, using a bromwich formulation," *J. Opt. Soc. Am. A*, Vol. 5, no. 9, p. 1427, 1988.

33. Lin, H. B., J. D. Eversole, and A. J. Campillo, "Excitation localization principle for spherical microcavities," *Optics Letters*, Vol. 23, no. 24, pp. 1051–1053, 1998.

34. Khaled, E. E. M., S. C. Hill, and P. W. Barber, "Internal electric energy in a spherical particle illuminated with a plane wave or off-axis gaussian beam," *Applied Optics*, Vol. 33, no. 3, pp. 524–532, 1994.

35. Khaled, E. E. M., S. C. Hill, and P. W. Barber, "Light scattering by a coated sphere illuminated with a gaussian beam," *Applied Optics*, Vol. 33, no. 15, p. 3308, 1994.

36. Dubreuil, N., J. C. Knight, D. K. Leventhal, V. Sandoghdar, J. Hare, and V. Lefevre, "Eroded monomode optical fiber for whispering-gallery mode excitation in fused-silica microspheres," *Optics Letters*, Vol. 20, no. 14, p. 1515, 1995.

37. Knight, J. C., G. Cheung, F. Jacques, and T. A. Birks, "Phase-matched excitationof whispering-gallery-mode resonances by a fibertaper," *Optics Letters*, Vol. 22, no. 15, p. 1129, 1997.

38. Serpengüzel, A., S. Arnold, G. Griffel, and J. A. Lock, "Enhanced coupling to microsphere resonances with optical fibers," *J. Opt. Soc. Am. B*, Vol. 14, no. 4, pp. 790–795, 1997.

39. Blair, S., and Y. Chen, "Resonant-enhanced evanescent-wave fluorescece biosensing with cylindirical optical cavities," *Applied Optics*, Vol. 40, no. 4, pp. 570–581, 2001.

40. Krioukov, E., A. Driessen, D. J. W. Klunder, J. Greve, and C. Otto, "Sensor based on an integrated optical microcavity," *Optics Letters*, Vol. 27, no. 7, pp. 512–514, 2002.

41. Ching, S. C., H. M. Lai, and K. Young, "Dielectric microspheres as optical cavities: Einstein a and b coefficients and level shift," *J. Opt. Soc. Am. A*, Vol. 20, no. 2, pp. 312–316, 1987.

42. Lai, H. M., S. C. Ching, and K. Young, "Dielectric microspheres as optical cavities: Thermal spectrum and density of states," *J. Opt. Soc. Am. A*, Vol. 20, no. 2, pp. 312–316, 1987.

43. Lai, H. M., P. T. Leung, and K. Young, "Limitations on the photon storage lifetime in electromagnetic resonances of highly transparent microdroplets," *Physical Review A*, Vol. 41, no. 9, pp. 5199–5204, 1990.

44. Lide, D. R., ed., *CRC Handbook of Chemistry and Physics*, C R C Press LLC, Boca Raton, 2000.

45. Sojka, B., P. A. E. Piunno, C. C. Wust, and U. J. Krull, "A novel phosphoramidite method for automated synthesis of oligonucleotides on glass supports for biosensor development," *Applied Biochemistry and Biotechnology*, Vol. 89, pp. 85–103, 2000.

46. Eggins, B. R., *Biosensors - An Introduction*, J. Wiley, Teubner, 1999.

47. Hacia, J. G., L. C. Brody, M. S. Chee, S. P. Fodor, and F. S. Collins, "Detection of heterozygous mutations in brca1 using high density oligonucleotide arrays and two-colour fluorescence analysis," *Nature Genetics*, Vol. 14, pp. 441–447, 1996.

48. Shoemaker, D. D., D. A. Lashkari, D. Morris, M. Mittmann, and R. W. Davis, "Quantitative phenotypic analysis of yeast deletion mutants using a highly parallel molecular bar-coding strategy," *Nature Genetics*, Vol. 14, pp. 450–456, 1996.

49. DeRisi, J., L. Penland, P. O. Brown, M. L. Bittner, P. S. Meltzer, M. Ray, Y. Chen, Y. A. Su, and J. M. Trent, "yuse of a cdna microarray to analyse gene expression patterns in human cancer," *Nature Genetics*, Vol. 14, pp. 457–460, 1996.

50. Head, S. R., Y. H. Rogers, K. Parikh, G. Lan, S. Anderson, P. Goelet, and M. T. Boyce-Jacino, "Nested genetic bit analysis (n-gba) for mutation detection in the p53 tumor suppressor gene," *Nuc Acids Res.*, Vol. 25, pp. 5065–5071, 1997.

51. Running, J. A., and M. S. Urdea, "A procedure for coupling of synthetic oligonucleotides to polystyrene microtiter wells for hybridization capture," *BioTechniques*, Vol. 8, pp. 276–277, 1990.

52. Southern, E., K. Mir, and M. Shchepinov, "Molecular interactions on microarrays," *Nature Genetics*, Vol. 21, pp. 5–9, 1999.

53. Z Guo, Z., R. A. Guilfoyle, A. J. Thiel, R. Wang, and L. M. Smith, "Direct fluorescence analysis of genetic polymorphisms by hybridization with oligonucleotide arrays on glass support," *Nucleic Acids Res.*, Vol. 22, pp. 5456–5465, 1994.

54. Kumar, A., O. Larsson, D. Parodi, and Z. Liang, "Silanized nucleic acids: a general platform for dna immobilization," *Nucleic Acids Res.*, Vol. 28, pp. E71–E71, 2000.

55. Maskos, U., and E. M. Southern, "Oligonucleotide hybridizations on glass supports: a novel linker for oligonucleotide syntsynthesizedybridization properties of oligonucleotides synthesised in situ," *Nucleic Acids Res.*, Vol. 20, pp. 1679–1684, 1992.

56. Lamture, J. B., K. L. Beattie, B. L. Burke, M. D. Eggers, D. J. Ehrich, R. Fowler, M. A. Hollis, B. B. Koskcki, R. K. Reich, S. R. Smith, R. V. Varma, and M. E. Hogan, "Direct detection of nucleic acid hybridization on the surface of a charge coupled device," *Nucleic Acids Res.*, Vol. 22, pp. 2121–2125, 1994.

57. Joos, B., H. Koster, and R. Cone, "Covalent attachment of hybridizable oligonucleotides to glass supports," *Anal.Biochem.*, Vol. 247, pp. 96–101, 1997.

58. Rogers, Y. H., P. Jiang-Baucom, Z. J. Huang, V. Bogdanov, S. Anderson, and M. T. Boyce-Jacino, "Immobilizaton of oligonucleotides onto a glass support via disulfide bonds: A method for preparation of dna microarrays," *Anal.Biochem.*, Vol. 266, pp. 23–30, 1999.

59. Bale, M. D., S. J. Danielson, J. L. Daiss, K. E. Goppert, and R. C. Sutton, "Influence of copolymer composition on protein adsorption and structural rearrangements at the polymer surface," *Journal of Colloid and Interface Science*, Vol. 132, pp. 176–187, 1989.

60. Company, P. C., "Double-agents cross-linking reagents selection guide," *Physica D*, Vol. 85, pp. 225–238, 2001.

61. Boom, R., C. J. A. Sol, M. M. M. Salimans, C. L. Jansen, P. M. E. W. van Dillen, and J. V. der Noordaa, "Rapid and simple method for purification of nucleic acids," *Journal of Clinical Microbiology*, Vol. 28, pp. 495–503, 1990.

62. Gingeras, T. R., D. Y. Kwoh, and G. R. Davis, "Hybridization properties of immobilized nucleic acids," *Nucleic Acids Res.*, Vol. 15, no. 13, pp. 5373–5390, 1987.

63. Haggin, J., "New applications touted for immobilized artificial membranes," *Chem. Eng. News*, Vol. 72, pp. 34–35, 1994.

64. Douglas, A. S., and C. A. Monteith, "Improvements to immunoassays by use of covalent binding assay plates," *Clin. Chem.*, Vol. 40, pp. 1833–1837, 1994.

65. Steel, A. B., R. L. Levicky, T. M. Herne, and M. J. Tarlov, "Immobilization of nucleic acids at solid surfaces: effect of oligonucleotide length on layer assembly," *Biophys J.*, Vol. 79, pp. 975–981, 2000.

66. Gregorius, K., and M. Thiesen, "In situ deprotection: a method for covalent immobilization of peptides with well-defined orientation for use in solid phase immunoassays such as enzyme-linked immunosorbent assay," *Anal. Biochem.*, Vol. 299, no. 1, pp. 84–91, 2001.

67. Vijayendran, R. A., and D. E. Leckband, "A quantitative assessment of heterogeneity for surface-immobilized proteins," *Anal. Chem.*, Vol. 73, pp. 471–480, 2001.

68. Cantarero, L. A., J. E. Butler, and J. W. Osborne, "The adsorptive characteristics of proteins for polystyrene and their significance in solid-phase immunoassays," *Anal. Biochem.*, Vol. 105, pp. 375–382, 1980.